POLITECNICO DI TORINO

Collegio di Ingegneria Chimica e dei Materiali

Corso di Laurea Magistrale
in Ingegneria Chimica e dei Processi Sostenibili

Tesi di Laurea Magistrale

CO_2 methanation using activated carbon derived from coconut shell biomass as support for Ni and Ni-Ce catalysts

Relatori

prof. Specchia Stefania
prof. Henriques Carlos Manuel Faria De Barros
Dr. Bacariza Rey Maria del Carmen

Candidato
Vitacchione Vittorio

Marzo 2023

Abstract

In this thesis, it was studied how an activated carbon, usually used for the purification of exhaust gases containing organic compounds such as VOCs (volatile organic compounds) or for water treatment, performs in the field of heterogeneous catalysis, loading Ni or Ni-Ce as active metal and acting as a catalyst for the methanation reaction. Three activated carbons were studied as supports, all derived from the same precursor (coconut shell), but activated by different methods such as physical activation with CO_2 and chemical activation with H_3PO_4 and $ZnCl_2$. Ni and Ni-Ce catalysts were prepared by incipient wetness impregnation and co-impregnation, respectively, and characterized by N_2 Adsorption, TPR, TGA, TEM, SEM. After assessing catalysts' properties in terms of hydrophobicity, textural properties or metallic dispersion, among all, catalytic tests were carried out, under conventional and aging conditions, at atmospheric pressure and temperatures between 240 and 450 °C (86100 mL h^{-1} g_{cat}^{-1}, H_2:CO_2 = 4:1). The type of activation procedure was found to modify the textural properties of the carbons, with CO_2-derived one exhibiting a purely microporous structure. In addition, the use of chemical agents for the synthesis led to the presence of residues in the carbons. In terms of Ni-catalysts, the best results were exhibited by the sample supported over the CO_2-derived carbon, which presented a higher basic character. Furthermore, the addition of Ce was found to boost the catalytic activity due to the improvement of the metallic dispersion and the promotion of carbon dioxide molecules activation on CeO_2 sites. Among all, the highest CH_4 yield (~80 % at 370 ºC) was obtained for catalysts with 20 wt.% Ni and 20 wt.% Ce deposited on H_3PO_4 and CO_2-derived activated carbons. The latter was chosen as the most outstanding due to the best compromise in terms of greener preparation conditions and superior performance, being also tested under aging conditions without a remarkable activity loss over the time. Also, the results obtained for the best catalyst from this thesis were comparable and/or superior to other catalysts with a carbon base or generally used for methanation.

SOMMARIO

La CO_2 è uno dei principali problemi ambientali di questo secolo, in quanto il suo rilascio nell'atmosfera e la sua concentrazione stanno aumentando sempre di più, causando il riscaldamento globale. Per porre rimedio al rilascio di anidride carbonica nell'atmosfera, si stanno studiando diverse soluzioni e quella discussa in questa tesi rappresenta una strategia non solo per il rilascio netto di CO_2 pari a 0, ma anche per lo stoccaggio di energia. Power-to-gas è una strategia che si realizza attraverso la reazione di Sabatier e mira a prelevare l'anidride carbonica in uscita dagli impianti di produzione o immessa direttamente in atmosfera attraverso soluzioni CCU e a farla reagire con l'idrogeno prodotto dall'idrolisi dell'acqua utilizzando fonti di energia rinnovabili. Tuttavia, sebbene questa reazione sia favorita a basse temperature e a pressione atmosferica, è necessaria la presenza di un catalizzatore per attivare le molecole di anidride carbonica, altamente stabili. I catalizzatori per questa reazione sono solitamente composti da Ni come metallo attivo, grazie alla sua grande disponibilità ed economicità rispetto a rodio, rutenio o palladio. Per quanto riguarda i supporti comuni, sono stati riportati ossidi metallici, zeoliti, silice mesoporosa o strutture metallo-organiche. Inoltre, pochi studi hanno riportato l'uso di carboni attivi. Per questi motivi, questa tesi intendeva valutare i carboni attivi derivati dal guscio di noce di cocco, un rifiuto biologico facilmente disponibile a causa del suo crescente consumo, come supporto per catalizzatori Ni e Ni-Ce da applicare alla metanazione della CO_2. I catalizzatori sono stati preparati mediante impregnazione/co-impregnazione a umido incipiente e caratterizzati con diverse tecniche avanzate. Infine, sono stati eseguiti test catalitici in condizioni convenzionali e di invecchiamento. Questa tesi è stata sviluppata nel laboratorio CATHPRO/CQE del dipartimento di ingegneria chimica dell'Instituto Técnico Superior di Lisbona. Il progetto si è avvalso della collaborazione di ricercatori della NOVA School of Science and Technology nel settore dei carboni attivi per il trattamento delle acque reflue, l'abbattimento dei composti organici volatili (VOC) e altre applicazioni correlate. I ricercatori della NOVA hanno fornito i carboni attivi, derivati dal guscio della noce di cocco, da utilizzare presso il dipartimento di ingegneria chimica del Técnico.

Lo studio ha riguardato la sintetizzazione dei catalizzatori mediante impregnazione/co-impregnazione a umido incipiente e caratterizzati con diverse tecniche avanzate, sono stati eseguiti test catalitici in condizioni convenzionali e di invecchiamento. Le tecniche di caratterizzazione hanno riguardato tutti gli 11 catalizzatori sintetizzati includendo: N_2 adsorption, SEM, TEM da cui derivata una distribuzione della dimensione delle particelle e della dispersione metallica, TGA da cui è anche stato calcolato l'indice di idrofobicità, XRD e TPR. I carboni attivi su cui caricare il principio attivo sono stati di tre tipi, tutti provenienti dallo stesso precursore ma attivati tramite attivazione chimica con $ZnCl_2$ (codice: AC_Z), H_3PO_4 (codice AC_H) e attivazione fisica con CO_2 (codice AC_C). Dopo una caratterizzazione preliminare, è stato scelto il carbone attivo sintetizzato utilizzando l'acido fosforico come agente chimico per studiare l'effetto del carico di Ni. Scelto un carico intermedio di Ni del 20 wt.%, anche gli altri due carboni attivi, preparati utilizzando $ZnCl_2$ e CO_2 per l'attivazione, sono stati impregnati di nichel. Infine, sono stati preparati catalizzatori NiCe con il 20 % di Ni e il 20 % di Ce sui tre supporti. Lo studio è iniziato caricando tramite impregnazione a umido incipiente una quantità di nichel di 2, 5, 10, 15, 20, 30% in peso, per individuare quale fosse il miglior catalizzatore in termini di conversione in modo tale da scegliere un carico ideale di nichel e caricarlo anche sulle altre due basi. Tramite una analisi iniziale è stato scelto come carbone attivo su cui caricare queste quantità di nichel, il carbone attivato con acido fosforico poiché presentava la maggior area superficiale e maggior volume dei pori rispetto alle altre due basi. Il lavoro è continuato caratterizzando questi catalizzatori, sintetizzati dopo una calcinazione a 500 °C per 3 ore, attraverso analisi TPR, TGA, XRD, adsorbimento di azoto concludendosi con

test catalitici per valutarne le performance in termini di conversione di anidride carbonica, selettività e resa a metano. Dopo una valutazione dei parametri sopracitati dei catalizzatori sintetizzati con AC_H, è stata scelta come quantità ideale di nichel, il 20% in peso, così da essere poi caricato sulle altre due basi ACc e ACz per valutarne le prestazioni.

Caratterizzazione dei carboni attivi

I carboni attivi sono stati ricavati da scarti di guscio di noce di cocco attivati attraverso processi chimici e fisici. I carboni attivi sono stati caratterizzati in primo luogo mediante analisi SEM, i cui risultati sono presentati in Figure 17, Figure 18 e Figure 19 per AC_H, AC_Z e AC_C, rispettivamente.

A partire dai risultati di AC_H (Figure 17), sono stati identificati alcuni contaminanti. In particolare, i picchi di fosforo sono stati i più intensi, con tracce di ferro, nichel, cromo e titanio, probabilmente dovute al processo di attivazione. La struttura del carbone risulta senza una forma definita. Nel caso di AC_z (Figure 18), è stata rilevata la presenza di zinco e cloro, probabilmente derivante dal processo di attivazione in cui è stato utilizzato $ZnCl_2$ come agente chimico. Per quanto riguarda la forma, si può osservare una struttura esagonale. Per ACc (Figure 19), il catalizzatore attivato con metodi fisici, cioè con anidride carbonica e ad alta temperatura e senza composti chimici esterni, si può notare che sono presenti solo contaminanti che fanno parte della struttura molecolare della noce di cocco. Infatti, sono stati trovati soprattutto potassio, silicio, sodio e alluminio, che sono costituenti della biomassa di cocco.

Sono state eseguite anche analisi termo gravimetriche in atmosfera di azoto per valutare la stabilità termica dei materiali (Figure 20). I risultati indicano che ACz e ACc sono stabili fino a 500 °C, mentre AC_H fino a 400 °C. Inoltre, una perdita di massa nella parte iniziale dell'analisi, intorno ai 150 °C, ha mostrato una perdita di acqua in tutti i campioni. Intorno ai 600 °C, la perdita di massa per AC_H e AC_C inizia ad aumentare drasticamente fino a raggiungere, alla fine dell'analisi, una perdita di massa del materiale del ~95%. Ciò indica che sono rimasti solo i contaminanti metallici del materiale. Infatti, come già visto nelle immagini SEM (Figure 17), è stata rilevata la presenza di ferro, cromo, nichel, titanio e fosforo per AC_H, mentre K, Si, Na e Al sono stati trovati in AC_C. Questi ultimi non sono in grado di decomporsi come il carbonio, poiché la loro temperatura di fusione è ben superiore a 800 °C ("Punti di Fusione dei Metalli | La Terra e il Fuoco," n.d.). Per quanto riguarda l'AC_Z, alla fine dell'intero processo ci sarà solo una perdita di massa del 20%.

Si è voluto inoltre valutare tramite TGA il comportamento dei tre carboni, in termini di perdita di peso, con l'aria come gas di analisi (Figure 21 e Figure 22). Inoltre, sono stati aggiunti gli andamenti delle analisi effettuate sotto azoto per confrontare i risultati in Figure 21. A causa del fatto che il carbonio brucia per l'ossigeno presente nell'aria a 550-700 °C ("Carbon | Facts, Uses, & Properties | Britannica," 2022) si verifica una perdita di massa significativa e più precoce rispetto all'azoto, più o meno alla stessa temperatura per tutti i carboni, a causa della reazione di ossidazione del carbonio a circa 550 °C. Come già detto, il carbone attivo non raggiunge una perdita di peso del 100%, poiché sono presenti contaminanti inorganici. Il fatto che il carbone attivo inizi a decomporsi già a 400 °C potrebbe portare, durante la fase di calcinazione dei catalizzatori a 500 ºC, a una percentuale effettiva di nichel sul catalizzatore superiore a quella nominale. Inoltre, come si può vedere seguendo le linee tratteggiate in Figure 22 a circa 500-600°C avviene la decomposizione isotermica. A causa del fatto che il carbonio inizia a bruciare e a rilasciare calore, è possibile notare che l'energia fornita dalla macchina per il campione, tra 500°C e 650°C, inizia a diminuire.

Per quanto concerne l'analisi XRD (Figure 23), si può notare che l'ampia banda a 20-35º è attribuita alla struttura amorfa del materiale. (Omri e Benzina, 2012). Inoltre, vi sono picchi attribuiti a contaminanti presenti nel carbone attivo. Ad esempio, i picchi di diffrazione situati a 10°, 26°, 31°, 34°, 36°, 47°, 37°, 40°, 56°, 61°, 62°, 68° e 72° corrispondono ai piani di riflessione (100), (002), (101), (102), (110), (103) e (112) della struttura esagonale dello ZnO per l'ACz, quello trattato con $ZnCl_2$ (Pellicano et al., 2017).

Per quanto riguarda i risultati dell'adsorbimento dell'azoto, presentati in Figure 24 e Figure 25 l'AC_H e l'AC_Z presentano proprietà testuali superiori all'AC_C sia in termini di volume dei pori che di area superficiale BET. Infatti, è stato possibile identificare l'andamento delle isoterme di Langmuir in Figure 24, cioè di materiali microporosi, pronunciati e confermati nel caso di ACc dove si può notare una frazione V_{micro} più elevata rispetto ai macropori. Per quanto riguarda AC_H e AC_Z è possibile associare le loro isoterme alle isoterme di tipo IV e V relative ai mesopori, in quanto questi presentano una percentuale di mesopori maggiore rispetto ai micropori. Inoltre, durante il desorbimento si verifica un'isteresi, che conferma senza dubbio la presenza di mesopori. Questi risultati non rispecchiano altre analisi di adsorbimento di N_2 riguardanti carboni attivi derivati da gusci di noce di cocco, in quanto quelli presentati in questa tesi sono di gran lunga superiori, ad esempio, a quelli presentati da (Gao et al., 2018). D'altro canto, per quanto riguarda gli altri supporti, i risultati di questo lavoro sono superiori a quelli ottenuti per la gamma-allumina in letteratura (Abate et al., 2016). Infine, dall'analisi della distribuzione delle dimensioni dei pori con il metodo BJH (Figure 25), si può confermare che i tre carboni attivi presentano prevalentemente micropori.

Infine, i valori di pHpzc sono stati forniti da FCT NOVA e presentati in Table 4.1. Questo parametro indica le proprietà acido-basiche del supporto, un parametro importante per la reazione di metanazione del CO_2. Come osservato, la basicità, proprietà favorevole all'attivazione del biossido di carbonio, ha seguito l'ordine: $AC_C > AC_Z > AC_H$.

Caratterizzazione catalizzatori al nichel

Considerando i risultati dell'assorbimento di N_2 e come già indicato nella sezione sperimentale di questa tesi, il carbone attivo che presenta le migliori proprietà testuali per disperdere efficacemente le particelle metalliche (AC_H) è stato scelto per ottimizzare il carico di Ni. A tal fine, sono stati testati contenuti di Ni dal 2 al 30 wt.%. Oltre a ciò, sono stati preparati anche catalizzatori con 20 wt.% di Ni supportati su carboni attivi AC_C e AC_Z. Le isoterme di adsorbimento per questa serie di catalizzatori sono presentate in Figure 26 e Table 4.2 verificando che il volume dei mesopori e le aree superficiali specifiche diminuiscono generalmente all'aumentare della quantità di nichel. Questi risultati sono attesi poiché l'aumento della quantità di carico porta inevitabilmente alla presenza di particelle sulla superficie e nei pori del carbonio. Da notare l'aumento dell'area superficiale specifica per $2Ni/AC_H$, $20Ni/AC_C$ e $20Ni/AC_Z$ rispetto ai loro supporti. In questi casi, si suggerisce che la calcinazione a 500 ºC effettuata per la decomposizione del nitrato di nichel abbia indotto anche un'apertura dei pori dei carboni per parziale decomposizione dei materiali, aumentandone l'area superficiale specifica.

Dalla distribuzione delle dimensioni dei pori presentata in Figure 27 si può notare che tutti i catalizzatori AC_H contengono micropori, la cui estensione si riduce all'aumentare del contenuto di Ni. Ciò potrebbe essere dovuto all'ostruire dei pori dovuto alle particelle di nichel.

L'obiettivo era anche quello di valutare se il nitrato di nichel si fosse decomposto durante il trattamento termico e, in effetti, si può vedere dalla Figure 28 che già intorno ai 350 °C si registra una perdita di massa dell'80%. Per correlare il legame del nitrato di nichel con il carbone attivo, è stata valutata anche la perdita di massa corrispondente al catalizzatore $15Ni/AC_H$ non sottoposto a calcinazione (85% intorno ai 500 °C). I tre andamenti dell'analisi sono stati poi correlati tra loro per quanto riguarda il catalizzatore $15Ni/AC_H$ non calcinato, la base AC_H e il nitrato di nichel utilizzato per impregnare il catalizzatore. Confrontando questi tre materiali, si può notare che il nitrato di nichel si decompone quasi completamente a 350 °C, mentre il carbone attivo (AC_H) mostra una diminuzione di peso ma non così rilevante a quella temperatura (350 °C), il che significa che la perdita di massa riscontrata nel catalizzatore $15Ni/AC_H$ non calcinato (85% a 500 °C) è attribuita interamente o quasi alla decomposizione del nitrato di nichel. Ciò conferma che, dopo la calcinazione a 500 °C, non dovrebbe rimanere alcun nitrato di nichel nei materiali.

In accordo con (Jovic et al., 2006), i picchi di diffrazione del Ni metallico (Ni^0) sono stati trovati nei catalizzatori di Ni a circa 45°, 53°, 78° (Figure 29), a dimostrazione che i carboni sono stati in grado di ridurre il nichel anche durante il trattamento termico in atmosfera inerte (azoto).

Per quanto riguarda l'H_2 -TPR, le variazioni del segnale TCD possono essere dovute al consumo di H_2 dovuto alla riduzione degli ossidi metallici o al rilascio di altri composti dai supporti di carbonio. In base ai risultati XRD precedentemente discussi, non è stata rilevata la presenza di NiO nei catalizzatori. Tuttavia, i risultati H_2 -TPR mostrati in Figure 30 e Figure 31 presentano variazioni del segnale TCD al di sotto dei 500 ºC. Infatti, mentre i picchi al di sotto dei 350 ºC potrebbero essere attribuiti a un sottilissimo strato di ossidi di nichel formatosi sulla superficie dei cluster di nichel metallico durante il contatto con l'aria, i picchi a temperature più elevate potrebbero essere attribuiti a una parziale decomposizione dei carboni attivi in atmosfera di idrogeno, in accordo con i profili ottenuti per AC_H, AC_Z e AC_C senza aggiunta di metalli.

In termini di risultati TEM, nella Figure 32 è possibile vedere che la superficie dei carboni attivi è generalmente omogenea e priva di particelle chiare. Inoltre, per quanto riguarda i diversi carichi di Ni su AC_H , si può vedere chiaramente dai risultati TEM in Figure 33, Figure 34, Figure 35 e Figure 36 che si formano particelle più grandi per contenuti metallici più elevati. Questo effetto potrebbe quindi spiegare la riduzione della superfice specifica e del volume dei pori con l'aumento della percentuale di Ni. Per quanto riguarda l'influenza del tipo di carbone attivo sulle dimensioni delle particelle metalliche, il confronto dei risultati TEM di Figure 36 ($20Ni/AC_H$), Figure 37 ($20Ni/AC_C$), e Figure 38 ($20Ni/AC_Z$) suggeriscono che tutti i materiali consentono una dispersione omogenea delle particelle di nichel metallico. Analizzando le micrografie TEM, sono state determinate le dimensioni medie delle particelle e delle dispersioni di Ni^0 (Table 4.3), essendo gli istogrammi presentati in Figure 39 e Figure 40. Come osservato, è stato confermato l'aumento delle dimensioni delle particelle con il carico di Ni. Inoltre, per quanto riguarda i catalizzatori con 20 wt.% di Ni, le particelle di Ni^0 più piccole e, di conseguenza, la più alta dispersione metallica sono state ottenute per 20Ni/ACc. La forma gaussiana ottenuta per gli istogrammi suggerisce inoltre che le particelle erano distribuite in modo omogeneo in termini di dimensioni in tutti i supporti.

Test catalitici per catalizzatori al nichel

I catalizzatori basati su AC_H e contenenti un carico variabile di Ni sono stati testati per primi, ottenendo le migliori prestazioni presentate in Table 4.4. Come osservato, nessuno dei materiali ha mostrato attività superiori al 5%. Questi risultati sono stati attribuiti a un effetto di avvelenamento delle impurità presenti nel supporto di carbone attivo. Tenendo conto di ciò, e in accordo con gli studi di letteratura in cui i carichi di Ni sono stati ottimizzati per altri tipi di supporti porosi come le zeoliti, è stato scelto un contenuto di Ni del 20 % in peso come il più favorevole. Considerando i catalizzatori con 20 wt.% di Ni e supportati sui tre tipi di carboni attivi, le migliori prestazioni catalitiche si riscontrano in Table 4.5. In effetti, il catalizzatore supportato su AC_C ha presentato i risultati migliori, in accordo con la maggiore basicità di questo supporto carbonioso e la più favorevole dispersione metallica. Anche in questo caso, l'attività e la selettività più scarse sono state fornite dal catalizzatore di carbonio AC_H, probabilmente a causa dell'impatto negativo delle impurità sulle proprietà del materiale. Infine, le prestazioni di $20Ni/AC_Z$ sono state inferiori a quelle di $20Ni/AC_C$ ma notevolmente migliori di 20Ni/AC$_H$. Ciò potrebbe essere dovuto alla basicità intermedia e alla dispersione metallica di questo campione.

I catalizzatori con un carico di Ni del 20 wt.% sono stati caratterizzati anche dopo il test con la XRD (Figure 41). È possibile notare che non ci si aspetta una notevole ri-ossidazione del nichel durante gli esperimenti, poiché non si osservano picchi di diffrazione aggiuntivi.

Caratterizzazione dei catalizzatori Ni-Ce

Partendo dai risultati di assorbimento di N_2 (isoterme in Figure 42 e proprietà testuali in Table 4.6), i risultati indicano che l'aggiunta di un secondo metallo porta a una riduzione delle aree superficiali e dei volumi dei pori. Anche in questo caso, ciò potrebbe essere attribuito al principio sopra menzionato secondo cui l'area disponibile diminuisce perché occupata dai cluster metallici.

Inoltre, un comportamento simile a quello dei catalizzatori monometallici di nichel si verifica per i catalizzatori drogati in termini di distribuzione delle dimensioni dei pori determinata con il metodo BJH (Figure 43). Infatti, con un secondo metallo si è riscontrato un volume di micropori ancora più ridotto a causa del blocco delle particelle, in questo caso sicuramente maggiore per la presenza delle particelle di cerio.

L'idrofobicità dei catalizzatori (tendenza a non trattenere acqua al suo interno o sulla sua superficie) è stata analizzata anche calcolando gli indici h (Table 4.7). In questo lavoro è stato di fondamentale importanza studiare questa proprietà sui catalizzatori, poiché l'acqua è un prodotto di reazione, allora se viene trattenuta sulla superficie del catalizzatore (bassa idrofobicità), la reazione sarà spostata verso i reagenti con una conseguente diminuzione della conversione. Se, invece, il catalizzatore ha un'elevata idrofobicità, l'acqua tende a lasciare immediatamente la superficie del catalizzatore, consentendo alla reazione di produrre immediatamente nuovi prodotti e quindi di spostare la reazione verso destra. Come si può vedere dalla Table 4.7 tutti gli indici h sono prossimi a 1, il che indica che tutti i catalizzatori sono altamente idrofobici. Pertanto, la reazione non dovrebbe essere fortemente inibita dalla presenza di acqua prodotta dalla reazione.

In termini XRD per i catalizzatori drogati con cerio (Figure 44), i picchi della ceria sono stati rilevati a 29°, 33°, 48° e 56°, in accordo con (Ghanbary e Jafarnejad, 2017) e (Abate et al., 2016). Inoltre, sono stati nuovamente osservati picchi di diffrazione del nichel metallico, indicando che anche il nichel è stato ridotto in questi campioni.

Inoltre, come precedentemente osservato per i catalizzatori di Ni, sono state rilevate variazioni del segnale TCD negli esperimenti H_2 -TPR (Figure 45 e Figure 46). Mentre i processi di riduzione al di sotto dei 350 ºC potrebbero essere attribuiti a uno strato di NiO sopra le particelle metalliche a causa del contatto con l'ambiente e i picchi al di sopra dei 400 ºC potrebbero suggerire la decomposizione del carbone attivo (soprattutto per AC$_Z$), non si può escludere la riduzione di specie di ceria ben disperse a ~400 ºC. Infatti, analizzando la Figure 46 in cui i catalizzatori Ni e NiCe sono confrontati con il corrispondente supporto di carbone attivo, è evidente la presenza di picchi più intensi nei campioni contenenti Ce per i tre carboni, probabilmente dovuti all'ulteriore riduzione di CeO_2 nell'intervallo di temperatura in analisi.

Come affermato da (Bacariza et al., 2018) e (Martin et al., 2019) e in accordo con i risultati TEM presentati in Figure 47, Figure 48, Figure 49 e soprattutto, Figure 47 le particelle di nichel ridotto tendono a diventare più piccole e meglio distribuite quando viene introdotto il cerio.

In base all'analisi delle dimensioni delle particelle, delle dispersioni metalliche e degli istogrammi (Table 4.8 e Figure 51), si conferma che l'aggiunta di Ce riduce le dimensioni delle particelle di Ni^0 migliorandone la dispersione. Infatti, si è verificata una diminuzione del diametro delle particelle di nichel quando si è confrontato il NiCe con i catalizzatori di Ni, corrispondente al 66% per 20Ni20Ce/AC_H, al 46% per 20Ni20Ce/AC_Z e al 50% per 20Ni20Ce/AC_C. Inoltre, si osserva chiaramente che quando si confrontano catalizzatori al cerio e non al cerio in Figure 51 l'istogramma tende a spostarsi verso dimensioni più piccole e la sua ampiezza tende a diminuire, risultando in un maggior numero di particelle con lo stesso diametro.

Test catalitici per i catalizzatori Ni-Ce e confronti

Le prestazioni catalitiche dei campioni contenenti 20 wt.% di Ni e 20 wt.% di Ce, così come i riferimenti di Ni monometallico, sono riportate nella Figure 52. Come osservato, e grazie alla capacità del Ce di ridurre le dimensioni delle particelle di nichel metallico e di attivare efficacemente la CO_2 (Bacariza et al., 2018) e (Martin et al., 2019), la conversione è passata da ~5% per 20Ni/AC_H a ~80% per 20Ni20Ce/AC_H . Infatti, sebbene tutti i catalizzatori drogati abbiano mostrato una conversione superiore al 70% a ~360 °C, il miglior catalizzatore drogato è stato quello supportato sul carbone attivo peggiore, con una conversione dell'80% a 360 °C. In termini di selettività a CH_4 (l'altro sottoprodotto è il CO in tutti i casi), è molto vicino al limite termodinamico, mentre in termini di resa, i migliori catalizzatori che presentano risultati molto simili sono il NiCe basato su AC_H e AC_C. È interessante notare che la selettività del metano diminuisce drasticamente con l'aumento della temperatura e l'assenza di cerio nel catalizzatore, mentre rimane molto alta e segue l'andamento della termodinamica nel caso dei catalizzatori drogati, confermando e addirittura superando i valori di selettività ottenuti da (Fujita e Takezawa, 1997).

Come per i catalizzatori di nichel monometallici, i risultati dell'analisi XRD per i campioni drogati al cerio dopo i test catalitici sono presentati in Figure 53. I diffrattogrammi non hanno mostrato alcuna formazione di ossido di nichel, suggerendo che non si è verificata una significativa ri-ossidazione delle specie di nichel durante gli esperimenti.

È stato inoltre eseguito un test di stabilità per 9 giorni su catalizzatore 20Ni20Ce/ACc. Mentre il giorno 1 e il giorno 9 è stato eseguito un test convenzionale a temperature variabili (risultati in Figure 54), gli esperimenti a lungo termine sono stati eseguiti per 6 h nei giorni da 2 a 8. Infatti, sono stati eseguiti test di 6 ore a ~350 ºC nei giorni 2, 3, 4, 5, 6 e 8, mentre un test a ~250 ºC è stato eseguito il giorno 7 (risultati in Figure 55).

Come si può vedere nella Figure 54 per tutti e tre i parametri, si è registrata una diminuzione dell'attività del catalizzatore, almeno per le temperature più basse, mentre già a partire da 350 °C la diminuzione della conversione, della selettività e della resa è stata di pochi punti percentuali. Infatti, il test di stabilità (Figure 55) a 350 °C mostra una perdita di conversione molto bassa del catalizzatore in 42 ore di attività, pari al 3%, e una selettività trascurabile.

Infine, il miglior catalizzatore di questo lavoro, 20Ni20Ce/AC_C , è stato confrontato con campioni della letteratura in Table 4.9. Tutti i catalizzatori sono stati testati a 1 atmosfera, ad eccezione del catalizzatore (Finestra et al., 2021), dove è stata scelta una pressione di prova il più possibile vicina a quella atmosferica (3 bar). Come verificato, il miglior catalizzatore di questa tesi presenta risultati comparabili o addirittura migliori rispetto a quelli della letteratura supportati su carboni o anche su altri tipi di materiali come gli ossidi misti.

In questa tesi è stato analizzato il potenziale dei carboni attivi derivati dal guscio di noce di cocco come supporto per il catalizzatore della reazione di metanazione del biossido di carbonio. A tal fine, sono stati studiati tre carboni, sintetizzati mediante strategie di attivazione chimica e fisica. Il nichel è stato scelto come metallo attivo, mentre è stato analizzato il ruolo del drogaggio dei campioni con Ce. Dopo una caratterizzazione preliminare, è stato scelto il carbone attivo sintetizzato utilizzando l'acido fosforico come agente chimico per studiare l'effetto del carico di Ni sui risultati. I risultati, ottenuti per contenuti di Ni da 2 a 30 wt.%, indicano che le particelle di nichel metallico erano più grandi con carichi più elevati e le proprietà testuali si riducevano sistematicamente a causa del blocco dell'accessibilità dovuto alle specie metalliche. Nonostante le dimensioni delle particelle inferiori a 25 nm per tutti i carichi di Ni, nessuno dei catalizzatori di Ni supportati su carbone attivo AC_H ha superato una conversione del biossido di carbonio di ~5%, essendo ciò attribuito alla presenza di impurità nel carbone derivanti dalla fase di preparazione e in grado di avvelenare o inibire i siti attivi.

Considerando un carico intermedio di Ni del 20 wt.%, anche gli altri due carboni attivi, preparati utilizzando $ZnCl_2$ e CO_2 per l'attivazione, sono stati impregnati di nichel. In questo caso, l'utilizzo del carbone attivo preparato per attivazione fisica con anidride carbonica ha portato alle migliori prestazioni sia in termini di conversione che di selettività, attribuite alla minore dimensione delle particelle di nichel e alla migliore basicità di questo campione.

Infine, sono stati preparati catalizzatori NiCe con 20 wt.% di Ni e 20 wt.% di Ce sui tre supporti. Il Ce, in accordo con la letteratura, è risultato in grado di ridurre significativamente le dimensioni delle particelle di Ni (riduzioni dell'ordine del 45-66%) e probabilmente di migliorare la capacità di attivazione del biossido di carbonio dei catalizzatori. Di conseguenza, dopo l'aggiunta di Ce è stato osservato un miglioramento dell'attività, particolarmente rilevante per il supporto AC_H, con conversioni di ~80% a 360 ºC. Il catalizzatore più importante, 20Ni20Ce/ACC, che ha mostrato risultati simili o migliori rispetto ad altri carboni e supporti presenti in letteratura, è stato anche sottoposto a un test di disattivazione a condizioni variabili per 9 giorni, essendo la stabilità promettente nel tempo.

Di conseguenza, questa tesi ha dimostrato l'idoneità della biomassa del guscio di cocco per la sintesi di promettenti supporti di carbone attivo per la reazione di metanazione della CO_2. Considerando i risultati ottenuti, studi complementari per analizzare la cinetica, completare la caratterizzazione dei campioni esausti o anche analizzare il meccanismo sui catalizzatori potrebbero essere potenziali studi futuri per completare i risultati ottenuti.

Index

Figures index

Table index

List of abbreviations:

SNG: Synthetic natural gas
RWGS: reverse water gas shift
CCU: Carbon Capture and Utilization
SEE or AC_H: Activated carbon activated with H_3PO_4
SE6 or AC_Z: Activated carbon activated with $ZnCl_2$
CH7 or AC_C: Activated carbon activated in a physical way with CO_2
VOC: Volatile organic compound
TPR: Temperature programming reduction
TGA: Thermo gravimetric analysis
TEM: Transmission electronic microscopy
SEM: Scanning electron microscopy

1. *Introduction*

CO_2 is one of the major environmental issues of this century, as its release into the atmosphere and its concentration are increasing more and more and causing global warming. To remedy the release of carbon dioxide into the atmosphere, a wide variety of solutions are being investigated, and the one discussed in this thesis represents a strategy not only to the net release of CO_2 equal to 0 into the atmosphere, but also to the storage of energy. Power-to-gas is a strategy that is carried out via Sabatier reaction and aims to take the carbon dioxide coming out of production plants or taken directly into the atmosphere via CCU solutions and make it react with hydrogen produced by hydrolysis of water using renewable energy sources. However, although this reaction is favoured at low temperatures and at atmospheric pressure, the presence of a catalyst is required to activate the highly stable carbon dioxide molecules. Catalysts for this reaction are usually composed of Ni as active metal due to its great availability and cheapness, when comparing to rhodium, ruthenium or palladium. Regarding the common supports, metal oxides, zeolites, mesoporous silica or metal-organic frameworks have been reported. In addition, few studies reported the use of activated carbons. For these reasons, this thesis intended the evaluation of activated carbons derived from coconut shell, a biowaste that is so readily available due to its ever-increasing consumption, as support for Ni and Ni-Ce catalysts to be applied in CO_2 methanation. Catalysts were prepared by incipient wetness impregnation/co-impregnation and characterized by a variety of advanced techniques. Catalytic tests were finally run under conventional and aging conditions.

This thesis was developed in the CATHPRO/CQE laboratory of the department of chemical engineering of Instituto Técnico Superior, in Lisbon. The project had the collaboration of researchers from NOVA School of Science and Technology from the area of activated carbons for wastewater treatment, Volatile Organic Compound (VOC) abatement and other related applications. NOVA researchers provided the activated carbons, derived from coconut shell, to be used at the chemical engineering department of Técnico.

2. *State of art*

2.1 Power to Gas

The energy production is one of the biggest problems in the last decade. During the last century it was produced by fossil fuel through a gas turbine or by burning dirty fuels from oil in thermal power plants and it is still produced in this way but the percentage of production is not anymore the same since the need for the reduction of CO_2 emission has pushed towards a creation of sustainable energy production plants that are developing all over the world as wind farms, hydroelectric power plants, photovoltaic camp, marine plant, geothermal and depending on the country it could be included nuclear plants too. They can allow for a significant production of energy power which could reach the half of total energy production, depending on the weather condition and the number of plants in the country.

The biggest problem of these sustainable power plant is the variability of surrounded conditions like wind, sun, rain that determine the quantity of renewable energy produced and production maxima doesn't coincide with the energy's demand the most of times. For example in a windy night or sunny day it is producing more energy that can be consumed by the citizen and it is necessary a storage of this energy's over production in order to reuse it for another time, otherwise it is necessary to stop or reduce the power of that power plants or even disconnect some photovoltaic or wind farm. It is requested to have a balance between demand and offer and this balance is possible just with a minimum of storage. It is possible to store energy in many ways, the storage depends on the place, on the investment and on the space's availability, it is developing technology like pumped hydro storage, compressed air energy storage, battery storage, thermal storage and many other that don't allow the flexibility and the capacity storage of a power to gas plant (Boudellal, 2018).

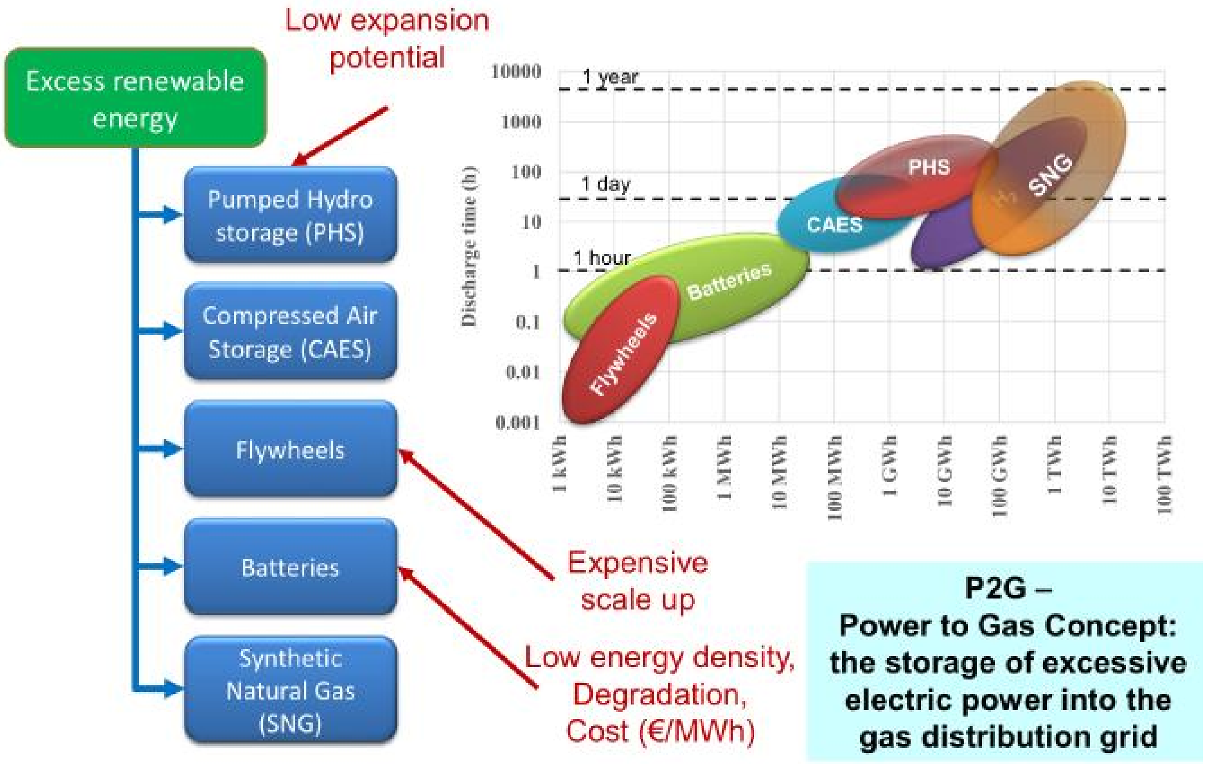

Figure 1 Possible solution for energy storage and capacity of storing of different methods, discharge time in hour as function of power. Adapted from (Schaaf et al., 2014)

The plant consists in an electrolyser which gets the energy from this unused energy, splitting oxygen and hydrogen that can be used in many ways for example putting these components directly in the industry or creating methane and injects it in the natural gas network. The technology to obtain oxygen and hydrogen can be different, for the moment it is used alkaline electrolysis and PEM (Proton Exange Membrane) but is starting to investigate high-temperature electrolysis (Boudellal, 2018). Scientists are looking for a discussed solution: power to gas. It allows a transformation of renewable energy in chemical bond energy, the renewable energy peacks coming for example from a windy day is used to get hydrogen from water through water hydrolysis.

This hydrogen can be injected directly in a natural gas network with a low concentration depending from the country starting from Belgium 0% in mol to Netherlands 12% in mol (Boudellal, 2018). This injection can affected the pipeline since hydrogen induces stress and corrosion of it and increases the safety risk during the transmission there could be degradation of performance of quality of industrial process because of these reason the pipe line has to be very specific made by specific material, for the transportation could be used the LOHC (liquid organic hydrogen carrier), components that reacts with hydrogen to get a liquid form for a safter and more economic transportation of it. Another possibility is the H_2 storage, it is developing thanks to tank storage or deep cave that allows higher pressure storage. The methanation is one of the most promising technology to be studied, the hydrogen reacts with CO_2 in order to obtain CH_4, an easier compound to be manage because it can be all injected directly in the existing natural gas network, and used as people are doing at the moment.

The more of the total methanation plant in Europe are developed in Germany with an actual production of 30,7 MW_{el}. A cost of production of hydrogen with PEM and alkaline electrolysis seen like an investment analysis was taken in consideration in order to evaluate if a power to gas plant will be more convenient in the future. After an evaluation of 153 projects in 22 country research tells that the price in producing hydrogen thus the overall cost of methanation will decrease until 2050, with a reduce in electrolysis cost of 75% and methanation of 67%. This reduction is due to the future automation and production capacity that are going to be increased but it would be better to use all the products of the plant to improve the economic efficiency as methane or hydrogen, oxygen or heat (M. Thema, 2019).

2.2 CO_2 methanation

Until few years ago the interest was on limiting the CO_2 emission demonstrated by Kyoto protocol and Paris Agreement, they focus the efforts on reduction of greenhouses emission. Nowadays the concept of CO_2 reduction is moving towards in CCU hence in Carbon Capture and Utilization concept. As a matter of facts, CO_2 from the exhaust gases of any process might be separated and it can be a carbon source as much as oil and coal, converting it in commodity or fuels. The lasts CO_2 capture technology are adsorption, absorption, membrane separation and chemical looping that can be integrated at the outlet of many factories for example in biomass/coal power generation, refineries or cement manufactures (Ashok et al., 2020). The problem of CO_2 is its stability, it is the final product of the most of reaction, one of the most stable components in the nature, though the methanation is favoured at lower reaction temperature between 25°C and 400°C but a proper catalyst is requested to achieve appropriate rate. One of the most used CO_2 fixation reactions is the methanation, the reaction for the thermodynamic is possible at ambient temperature and pressure but it doesn't start. Catalyst is the key of this process not only they increase the velocity of the reaction but catalysts will avoid the formation of unwanted species as coke and carbon monoxide, they increase selectivity, otherwise it allows to overcome the kinetic barrier in order to let start the process which otherwise would not happen despite it is thermodynamically favoured.

$$CO_2 + 4H_2 \leftrightarrow CH_4 + 2H_2O \quad (\Delta H_{298k} = -165\ KJ / mol) \tag{1}$$

$$CO_2 + 2H_2 \leftrightarrow C + 2H_2O\ (\Delta H_{298k} = -90{,}1\ KJ\ mol^{-1}) \tag{2}$$

$$CO_2 + C \leftrightarrow 2CO\ (\Delta H_{298k} = 172{,}4\ KJ\ mol^{-1}) \tag{3}$$

$$CO_2 + H_2 \leftrightarrow CO + H_2O\ (\Delta H_{298k} = 41{,}2\ KJ\ mol^{-1}) \tag{4}$$

$$CO_2 + CH_4 \leftrightarrow 2CO + 2H_2O\ (\Delta H_{298k} = 247{,}3\ KJ\ mol^{-1}) \tag{5}$$

2.1.1 Thermodynamics

It is interesting to study how conversion and selectivity change with temperature and pressure, looking at Gibbs free energy it is interesting to notice that it is 0 or less under 600°C and thus the reaction is spontaneous (-130,8 KJ/mol) (Strucks et al., 2021) but it will never happen without a catalyst that's why it is required. The reaction will be spontaneous when $\Delta G = 0$ and in this case it will have a temperature of 600°C, but the process is shifted through the products otherwise methane and water are going to be more favoured with a $T < 600°C$ because $\Delta G < 0$. As consequences of a decreasing in volume, as much the temperature is lower as much reaction will be favoured (*Le Chatelier's* principle), thanks to its exothermicity infact in this reaction, as much the temperature is lower as much the reaction will be favoured (ΔH_{298k} = -165 KJ / mol). In the case of ambient pressure, the reaction temperature should be less than 350°C in order to reach conversion higher than 90% and good methane selectivity otherwise the *reverse-water-gas-shift* (RWGS) will be favoured producing CO as a by-product, this CO would induce the Bouduard reaction resulting in formation of coke (Li et al., 2022).

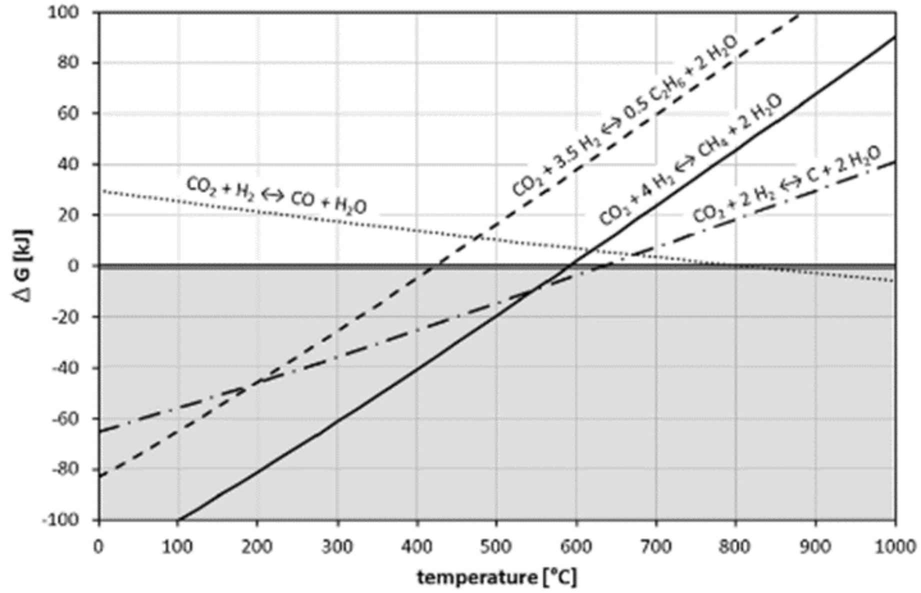

Figure 2 Delta Gibbs free energy as function of temperature for mains reaction involved in methanation

The expected reaction is $CO_2 + 4H_2 \leftrightarrow CH_4 + 2H_2O$ (ΔH_{298k} = -165 KJ / mol), this is the reaction moving on all the process, the ideal proportion is $H_2:CO_2 = 4:1$ if it will have less hydrogen, there will be coke and hydrocarbons formation (Mebrahtu et al., 2019).

Table 2.1 Thermodynamic of methanation at 1 bar

Thermodynamic		
T (ºC)	**Conv. (%)**	**Select. (%)**
150	**99,55**	**99,999913**
200	**98,75**	**99,9997984**
250	**97,10**	**99,9979393**
300	**94,20**	**99,9815054**
350	**89,69**	**99,8756804**
400	**83,48**	**99,3495714**
450	**76,07**	**97,2434335**
500	**68,94**	**90,4845043**

At 1 bar a compromise between thermodynamic and kinetics should be found at lower temperature thermodynamic drives the reaction forward but the kinetics is very low, instead in the opposite situation at higher temperature the kinetics is high but the conversion is lower (69% at 500°C) because of the thermodynamic.

Apart the influence of temperature it is interesting to consider as well, the dependence of pressure in order to evaluate in a future the right compromise to have a good conversion and a reasonable cost of investment. Starting from 1 bar until 30 bar and working in a favoured range of temperature reaction (200-550°C) the conversion will be always higher at higher working pressure, even the pressures values lead the process to high methane yields (Schmider et al., 2021). The ideal condition would be a temperature as low as possible and a pressure as high as possible, for example with a temperature of 200°C and a pressure of 30 bar the conversion of the reaction is near to 100%.

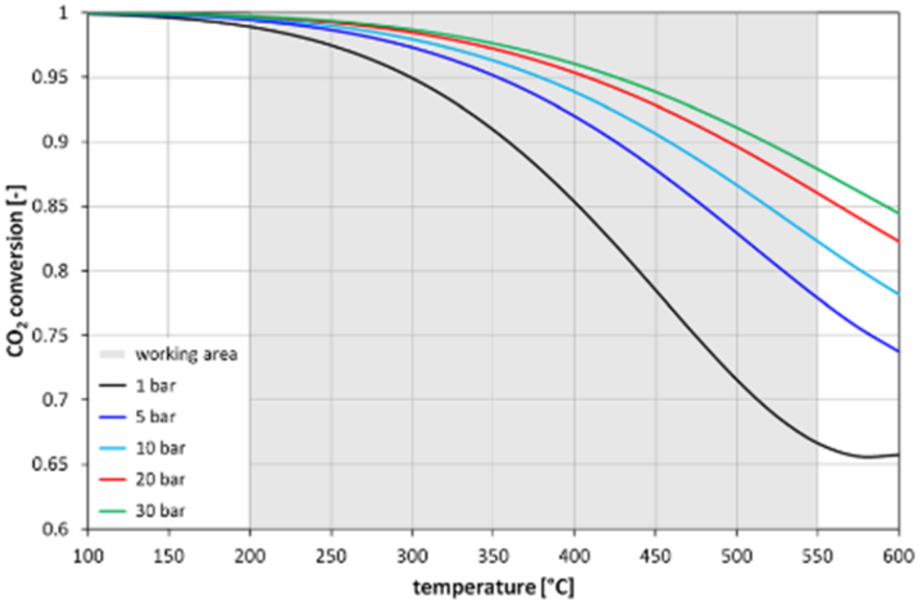

Figure 3 CO_2 conversion as a function of temperature, at different pressures. Adapted from (Schaaf et al., 2014)

2.1.2 Mechanism of reaction

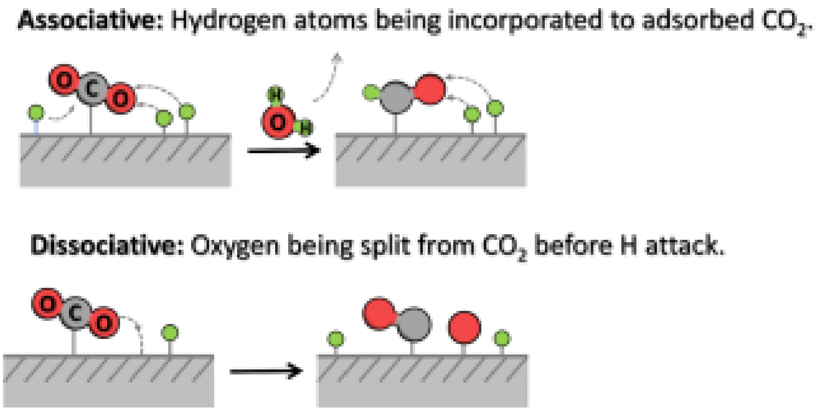

Figure 4 Possible alternative pathways leading to methanation. Adapted from (Jurca et al., 2021)

The mechanism of methanation, overall for Ni based catalysts, have been widely studied and researcher are not according everybody for a specific mechanism for CO_2 methanation, instead for CO mechanism, experimental findings support to a CO associative mechanism in order to form a carbide species on the surface of the catalyst and it competes with a dissociative H_2 adsorption (Schmider et al., 2021). The most of people are according that the CO_2 methanation is followed by a CO mechanism after the scission of one oxygen from the molecule and then it follows the pathways of CO mechanism. (Schmider et al., 2021).

For each catalyst it has been studied different way to react, different step of reaction and by-product with different mechanism of reaction and every catalyst would have its proper mechanism but the mechanism are mostly divided in two family. The first one speak about a CO_2 methanation forming CO as an intermediate product and subsequent CO methanation. The second one follows the direct hydrogenation of CO_2 without forming carbon monoxide as an intermediate product (Strucks et al., 2021).

The more spoken mechanism could be described by a combination of methanation and RWGS

$$CO_2 + H_2 \leftrightarrow CO + H_2O\ (\Delta H_{298k} = 41{,}2\ KJ\ mol^{-1}) \qquad RWGS$$

$$CO_2 + 4H_2 \leftrightarrow CH_4 + 2H_2O\ (\Delta H_{298k} = -165\ KJ\ /\ mol) \qquad methanation$$

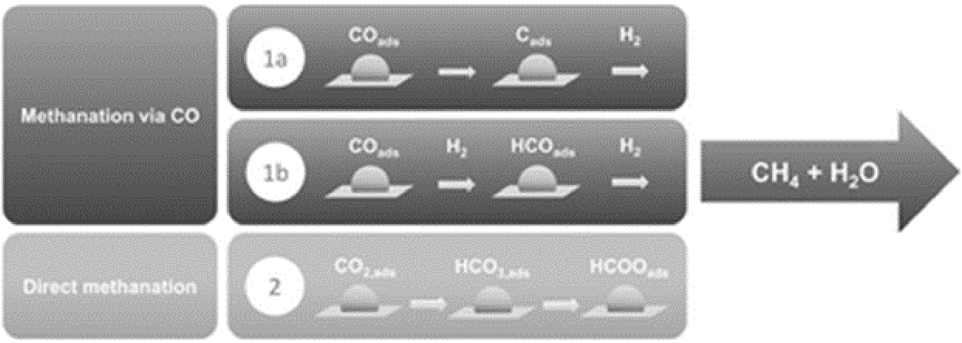

Figure 5 Different possible pathways for methanation. Adapted from (Strucks et al., 2021)

In a first step CO_2 dissociates on the catalyst surface's forming CO_{ads} and O_{ads} and it can either easily follows another dissociation forming carbon and oxygen or follows CO methanation. The carbon staying on the surface can, step by step, add hydrogen to form at the end CH_4 at the same moment the oxygen adsorbed on the catalyst can be hydrogenated and molecule of water will desorb from the surface. RDS of the reaction might follows two components: dissociation of adsorbed CO or the formation of CHO before being hydrogenated to CH_4. Besides the reaction involved, it could be present other reaction that can lead the selectivity to methane and they can form carbon or hydrocarbon following the boudouard reaction or exothermic pyrolysis (Strucks et al., 2021).

Only few works about the second mechanism explain CO_2 methanation occurs by a formation of carbonates, instead of CO as by product, being directly hydrogenated to became methane(Aldana et al., 2013). CO_2 adsorbs in an associative way on the surface of the catalyst and it reacts with detached hydrogen (H*) thanks to Ni^0. In the study of Aldana et all (Aldana et al., 2013) in the catalyst Ni/Ce/Zi for example carbon dioxide is activated thanks to Cerium/Zirconia making CO_3^{2-} meeting the hydrogen, it will form $HCOO^-$ before forming methane. This study will conclude that CH_4 and CO will have been formed by different mechanism and it is possible to consider CO as a subproduct of CO_2 reduction on Ce^{3+}.

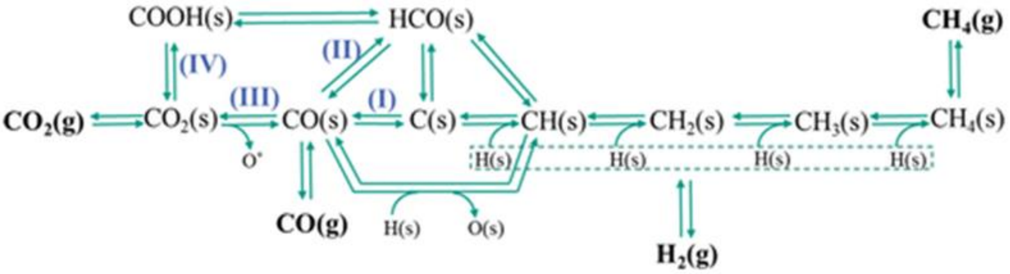

Figure 6 Possible reaction intermediaries for methanation. Adapted from (Schmider et al., 2021)

2.1.3 Catalysts

Many characteristics of a catalyst metal based might be influenced by different reasons: catalysts made by different metal precursors salt, by different particle size, content of active metal, the structure and chemical state of metal or the location of active sites (Li et al., 2022). The most used active metal in the methanation is nickel due to its high activity, cheaper price and availability.

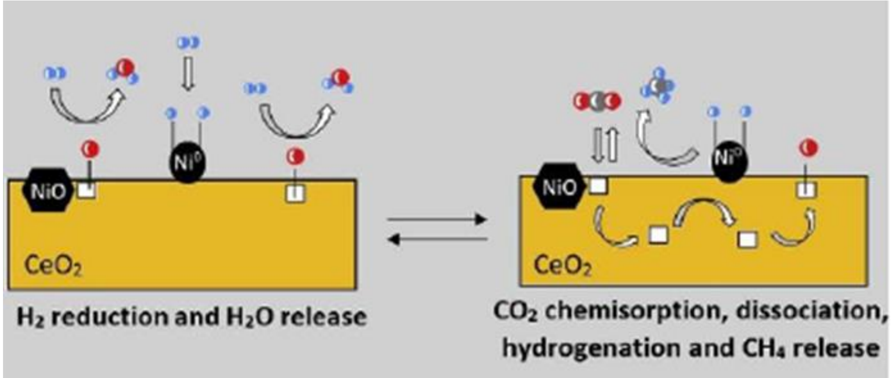

Figure 7 Reaction mechanism of Ni^0. Adapted from (Bacariza et al., 2020)

This is an easy availability and economic component that's why Ni-based catalyst is the most used in CO_2 methanation. It has been observed that due to defects in the structure of nickel oxide, once reduced it is able to adsorb and activate the methanation reagents, making it excellent for this reaction (Abu Bakar et al., 2012). Furthermore, it was observed by how Ni manages to radically change its performance when doped with Ce, in fact, thanks to the cerium, the Ni particles on the substrate are scaled down and it is clear that there is better dispersion. Furthermore, the nickel-cerium combination seems to be one of the best as nickel is responsible for the dissociation of hydrogen, and needs the association of a compound that adsorbs and activates CO_2 indeed cerium is responsible for the activation of carbon dioxide (finestra et al., 2021). Furthermore, as (Dzakaria et al., 2021) has shown, the successful coupling could also be due to the fact that the cerium particles enhance the reduction capabilities of nickel oxide.

Ruthenium

Ruthenium is one of the most selective and active catalyst for methanation reaction. Its behaviour depends on the ruthenium loading, it was investigated Ru/Al_2O_3 from 1% to 5% of ruthenium percentage (optimal at 4%), it should increase the basicity of the surface in such a way to form new CO_2 adsorption site therefore greater CO_2 conversion as much as the size of Ruthenium particle that increase the CH_4 selectivity. Many other bases have been studied as CeO_2, ZrO_2 and TiO_2, these are based catalysts with oxygen vacancy but also SiO_2 and Al_2O_3 without oxygen vacancy. From all of Ruthenium based catalyst the Ru/TiO_2 has been showed the most selectivity in CO_2 methanation and of this the rutile-type exhibited better dispersion thus more CH_4 selectivity and higher thermal stability (Ashok et al., 2020).

Rhodium

For this component as much as Ruthenium, the particle size influences the activity of the catalyst at lower temperature (135°C – 150°C), especially for bigger particle is increased the turnover frequency for CH_4 formation thanks to larger lateral faces of them otherwise at higher temperature the particle doesn't have influences on catalytic performance between 180°C and 200°C. As for the ruthenium the support TiO_2 is the best choice for the rhodium, it has been seen that the interaction with Ti^{3+} and the adsorbed CO could let happen the breaking of C-O bond (Ashok et al., 2020). A good results also come from Al_2O_3 that is the most common support for CO_2 methanation (Bacariza et al., 2020). This complex makes a chemical change of chemical state of rhodium forming a linear Rh-CO species and RhO_x resulting from CO_2 dissociation thus it helps the dissociation of molecule and increases the formation of CH_4 (Ashok et al., 2020).

Palladium

Palladium is able to make a dissociation of H_2, the H species is essential to produce more methane but a percentage above 5% has the tendency to let remain stable the multi-bond and CO species on the catalyst thus the reaction will decrease its velocity. Although a lot of work has been done, palladium does not perform well in terms of price-quality because it is unquestionable that it can be used as the sole active ingredient on a carrier because of the cost, but using it as a dopant for a main active ingredient such as Ru, as has been done by (Sharma et al., 2011), even though it provides a very high selectivity (99%), conversion is not high (55%).

For methanation, many catalysts are being studied, but even more so are catalysts with percentages of different components, such as Co-Fe (Jurca et al., 2021), or palladium-iron (Luo et al., 2020) and many other catalysts on many different bases, and attempts are being made to find the right combination of the different composition of the active ingredient, its spatial structure and its arrangement on an optimal base for all these combinations. Then, in recent times, attention is starting to be focused on activated carbon in terms of the basics. They have a very high surface area, much higher than the carriers studied so far such as Alumina or Titania, and attention is also being focused on activated carbons derived from biomass, which has a twofold advantage.

2.3 Activated carbons

Figure 8 Classic form of an activated carbon

Activated carbon, an amorphous form of carbonium, has the same composition of graphite but with a random and imperfect structure that allows a high specific surface, up to 2000 m^2/g and high porosity (Suhas et al., 2007). This characteristic is just one of the reasons why it is involved for example in outlet gas purification or water depuration, in effect it has the highest capacity to physically adsorb a component on its surface ("Activated Carbon," 2023). Activated carbons are among the oldest substances to be discovered for their ability to adsorb pollutants from liquid and gaseous streams. Pollutants can be of various kinds, we can find organic or inorganic substances. We can generally divide them into two types depending on the diameter of the granules from which they are composed. In fact, we can define PAC (powdered activated carbon) and GAC (granular activated carbon), from which we can well derive the consequences of having one type rather than another, for example difficulty in diffusion, lower or higher pressure drops or more or less difficulty in regeneration depending on which one is chosen (Suhas et al., 2007).

2.3.1 Synthesis of activated carbon

The original material for an activated carbon could be from different nature, the most are deriving from natural component as lignocellulosic biomass: coconut shell, pistachio nutshell, palm kernel shell, nutshell, wood then peat and coal but materials from different origin have been studying and for each specific derived material, the pore size distribution and the process to have it, could be different, but the overall procedure follows two mainly different steps. The first one is the carbonization, a thermal treatment reaching high temperature (800°C maximum) with the absence of oxygen, this process is then followed by an activation of the obtained carbon that might divided into two pathways, chemical and physical activation (Mohamad Nor et al., 2013).

Carbonization

By a thermal decomposition it is going to take out the non-carbon species, but a low-heating rates (10-15°C/min) has to take place otherwise the volatilization and low char yield will be obtained. Higher temperatures increase fixed carbon and ash content and a better quality of char will be reached, independently from the origin of the material and precursors composition the microporosity will be the same (Mohamad Nor et al., 2013). In addition, this part is characterised and carried out by a pyrolysis process whereby temperatures are raised to around 800°C-1000°C in order to produce charcoal, which is then followed by an activation process using carbon dioxide or oxygen.

$$Carbon\ yield\ (\%) = \frac{AC\ weight}{raw\ material\ weight} \times 100 \tag{6}$$

Activation

With carbonization a first step of porosity has taken place into the carbon but the goal of activation is to enhance the volume porosity. There are three ways in order to activate carbons: physical, chemical and physiochemical activation (Lozano-Castelló et al., 2001). Physical activation might be made by steam, nitrogen, air, CO_2, letting flow these components in the carbon, they will gasify the most reactive carbons atoms in the structure in a selectively way, leaving empty spaces and the pore distribution will be created. For chemical activation it is used many chemical agents as zinc chloride, phosphoric acid, alkaline metal compounds, an example could be KOH, used to make active precursors of coal or char, in fact these chemical agent will be part of the structure of carbons in this way after the heating treatment, reaching higher temperature, the agent will be decomposed leaving much more porosity than the physical activation. The mains advantages of this type of activation are the lower temperatures taking place, shorter time needed and more carbon yield thanks to chemicals that avoid the formation of volatile compound and tar because of their dehydrogenation properties (Lozano-Castelló et al., 2001).

2.3.2 Application of activated carbon

Activated carbon is one of the most used compounds to purify water, gas and everything having ppm of organic and inorganic pollutant. Their properties as adsorption, depend on the treatment it was subjected to: physical or chemical activation, it could depend on the precursors or on the chemical used either on the gasification time (Omri et al., 2013). They are used in a wide variety of ways, in some studies activated carbon from lignin was applied to remove carbon monoxide from a stream (Suhas et al., 2007), or in (Molino et al., 2022)'s work, various activated carbons were used to purify biogas from siloxanes and H_2S. In the industrial sector, on the other hand, activated carbons are widely used. In general, their capacity is limited to adsorbing similar species, so polar materials will be very difficult to retain, and the contact time required depends on the size of the particles, i.e. whether we have GAC or PAC.

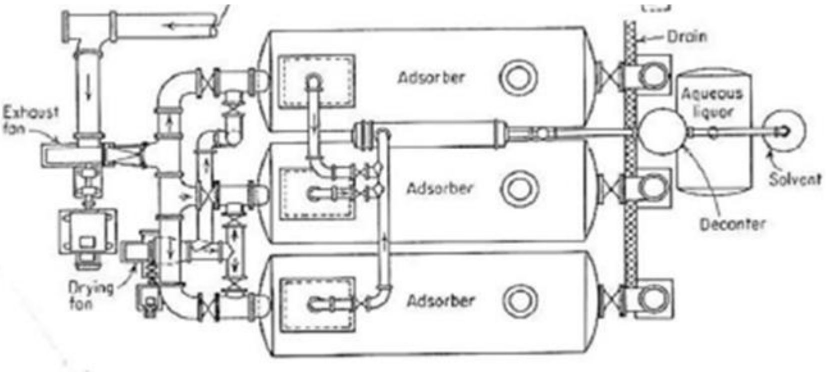

Figure 9 Solvent recovery adsorption plant. Adapted from (Specchia, 2022)

One industrial application is that of the fixed bed, where liquid or gas full of contaminants is made to flow so that it is retained by activated carbon, which will reach saturation and need to be regenerated. Or it is used for the recovery of very expensive solvents that cannot be thrown away, for example in a three-reactor scheme, where adsorption takes place in one, steam regeneration in the second and drying in the last, so that the process runs continuously. There are systems capable of dehumidifying the air by means of fixed beds of this material, where the air is forced to pass through a fixed bed of activated carbon creating a dry current at the outlet, or else systems where we can introduce dirty water, which passes through the bed, until it reaches the bottom of the tank. At the bottom, we have a series of pipes for the purified water, while the activated carbon continues to absorb pollutants. All these systems are developed in industry in the most diverse ways and for the most diverse purposes (Specchia, 2022).

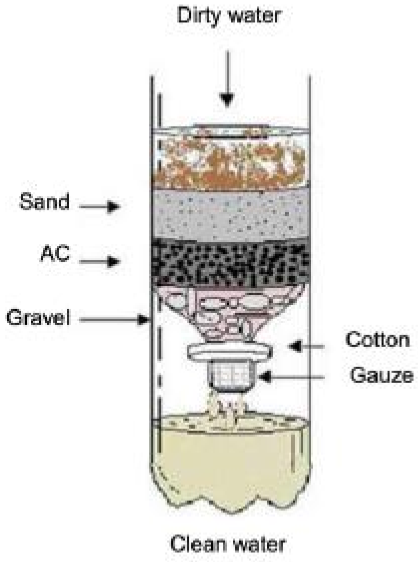

Figure 10 Water cleaning process with activated carbon. Adapted from (Specchia, 2022)

2.3.3 Activated carbon for CO_2 methanation

The study of activated carbons on which to deposit clusters of active ingredients such as ruthenium, rhodium or nickel is still ongoing. Very few activated carbons have been studied for this purpose, even more so activated carbons from biomass. For example, it was studied by (Swalus et al., 2012) how a catalyst known to be ideal for methanation, such as Rh/alumina, could be flanked by a catalyst that is excellent for hydrogen dissociation, such as Ni/activated carbon. The combination of these two catalysts resulted in 100% selectivity but not as high a conversion, since it was noted that thanks to the nickel and activated carbon, there was a diffusion of the hydrogen dissociated towards the flanked rhodium/alumina catalyst. Another study carried out by (finestra et al., 2021) showed the effect of an activated carbon (plant-derived biochar, depured with N_2 and activated with CO_2) doped with ceria on which Ni was deposited in a fixed concentration of 40% and to which cerium was added in gradually increasing concentrations, ranging from 10% to 40%, it has been noted that conversion is practically nil without cerium and increases as its concetration increases.

2.4 Goal of the thesis

This coupling of nickel and nickel cerium on activated carbon is very rare in the literature, which is assumed to have been very little studied, and moreover nickel placed on an activated carbon made from coconut waste. So the aim of this thesis is to investigate how the coupling of these components carries out the methanation reaction, studying the conversion, selectivity, yield and durability over time, after determining all the characteristics of this new catalyst that has been little studied, if at all. The use of coconut shell in order to valorise a waste is stepping more and more in everyday life thanks to the healthy properties that this fruit is offering. Everything concerning the affinity between these compounds will be studied, the acidity, the hydrophobicity, how the nickel and nickel cerium will dispose on the surface of carbon and how they are going to move on the reaction depending from the concentration in weight of nickel and then nickel doped with CeO_2.

3. Experimental section

3.1 Catalysts preparation

Three activated carbons used in this thesis were provided by FCT NOVA researchers. They were prepared using as raw material coconut shell (agricultural residues) collected from industries around Maceió – AL, Brazil. Coconut dried shells were previously ground and sieved in order to obtain a particle size between 1 and 3 mm. Two activated carbons were obtained by chemical activation with zinc chloride ($ZnCl_2$) and phosphoric acid (H_3PO_4). The particles were impregnated with the chemical agents (each separately) using an impregnation ratio (x_{ca}) of 2.5 (w/w) and were kept at 80 ºC for 4 h. Pyrolysis was then carried out under constant nitrogen flow (5 L/h). The temperature was raised at 5 ºC/min up to 600 ºC ($ZnCl_2$) and 450 ºC (H_3PO_4) and was maintained for 3 h. After that, all the samples were then washed with distilled water to remove excess of reagent and dried at 105-110ºC for 24 h. The activated carbons obtained by impregnation with $ZnCl_2$ were previously washed with HCl solution (2 N). A third activated carbon was obtained by physical activation with CO_2. The residues were firstly carbonized up to 800 °C (2 °C/min) under constant nitrogen flow (5 L/h) and maintained for 4 h. After cooling down to room temperature, they were subsequently heat treated under a CO_2 flow (1 L/h) at 800 °C (2°C/min) and maintained for 4 h. Table 3.1 summarized the preparation conditions and designations for these three samples. Activated carbons were grounded and sieved to obtain a particle size below 100 mesh.

Table 3.1 Main preparation conditions of the activated carbons used in this thesis and provided by FCT NOVA researchers.

Carbon	**Activation agent**	**Temperature (ºC)**	**Impregnation ratio (w/w)**
ACz	**$ZnCl_2$**	**600**	**2.5**
ACc	**CO_2**	**800**	**--**
AC_H	**H_3PO_4**	**450**	**2.5**

After collecting N_2 isotherms from the three carbons, the one with the highest specific surface area and pore volume, AC_H, was chosen for testing the influence of the Ni loading on the catalysts' properties and performances. Thus, 2, 5, 10, 15, 20 and 30 wt.% of nickel (nominal loadings) was incorporated over this activated carbon by incipient wetness impregnation method, the most widely used technique for heterogeneous catalysts preparation. This technique allows a metal nitrate (nickel nitrate in our case) to be dissolved in a solvent, in this case 2-propanol, so that the dissolved nitrate can easily enter the pores and then be subjected to a drying and calcination processes so that the solvent can evaporate and release the metal nitrate into the surface of the activated carbon (Sietsma et al., 2006).

For the deposition of the catalyst on the surface of the activated carbon, an amount of nickel nitrate ($NiNO_3*6H_2O$ from Sigma-Aldrich) corresponding to the desired weight percentage on the catalyst was dissolved in 2-propanol solvent (2-PrOH from Scharlau), using a volume close to carbon pore volume. Through a drop-by-drop deposition process combined with stirring, the impregnation solution was incorporated on the activated carbon. Afterwards, the material was placed in an oven at a temperature of 80 °C overnight. Finally, a calcination treatment was carried out under nitrogen flow for the decomposition and in-situ formation of nickel particles over the catalysts. Indeed, based on literature, is known that carbon is able to reduce the nickel nitrate into metallic nickel by itself. The calcination setup was composed by an oven and a fluidized bed reactor, set for an incipient fluidization to avoid the catalyst outgoing from the reactor and guarantee an homogeneous heat distribution. The calcination conditions, presented in Figure 11, were the following: ramp of 5 °C/min until the achievement of 500 °C followed by 3 hours at this temperature under an N_2 flow.

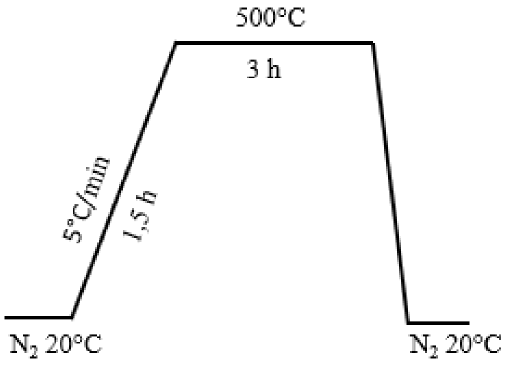

Figure 11 Temperature program used for calcination.

After identifying the best Ni nominal loading, 20 wt%, equivalent catalysts were prepared supported over AC_Z and AC_C carbons, following the same protocol previously described. Finally, three Ni-Ce catalysts were prepared containing 20 wt% of Ni and 20 wt.% of Ce (nominal loadings) by incipient wetness co-impregnation and again using the same conditions described above.

To sum up, the main preparation conditions of the catalysts from this work are presented in Table 3.2, Table 3.3 and Table 3.4 for AC_H, AC_C and AC_Z carbon supports, respectively.

Table 3.2 AC_H-based catalysts preparation parameters.

AC_H	**2Ni/AC_H**	**5Ni/AC_H**	**10Ni/AC_H**	**15Ni/AC_H**	**20Ni/AC_H**	**30Ni/AC_H**	**20Ni20Ce/AC_H**
Ni (wt.%)	2	5	10	15	20	30	20
Ce (wt.%)	0	0	0	0	0	0	20
Support mass (g)	0,78	0,76	0,72	0,68	0,64	0,56	0,90
Ni salt mass (g)	0,0805	0,20	0,4024	0,6036	0,8048	1,2072	1,5090
Ce salt mass (g)	0	0	0	0	0	0	0,9391

Table 3.3 AC_C-based catalysts preparation parameters.

AC_C	**20Ni/AC_C**	**20Ni20Ce/AC_C**
Ni (wt.%)	20	20
Ce (wt.%)	0	20
Support mass (g)	1,20	0,90
Ni salt mass (g)	1,5090	1,5090
Ce salt mass (g)	0	0,9391

Table 3.4 AC_Z-based catalysts preparation parameters.

AC_Z	**20Ni/AC_Z**	**20Ni20Ce/AC_Z**
Ni (wt.%)	20	20
Ce (wt.%)	0	20
Support mass (g)	1,20	0,90
Ni salt mass (g)	1,5090	1,5090
Ce salt mass (g)	0	0,9391

3.2 Characterization techniques

3.2.1 N_2 Adsorption

Thanks to this characterization technique it is possible to understand the total pore volume and the specific surface area of the catalyst. A molecule of N_2 occupies 0,162 nm^2 (Russo, 2022) thus knowing how much molecules it is adsorbed it is able to know the quantity of the specific surface m^2/g seeing from the graph when it will be the saturation of monolayer, furthermore it will be presented isotherms of adsorption and desorption, depending on the graph it can see which pores the catalyst has and depending on the hysteresis it is easy to understand the main shape of pores. It is possible to know specific surface through this formula:

$$\boldsymbol{S = n * A * N} \tag{7}$$

where **n** is the N_2 moles adsorbed on surface as monolayer, **A** is the m^2 of N_2 molecule, **N** is the Avogadro number. The machine has two different parts: the depuration and adsorption part, indeed before doing this adsorption is mandatory the cleaning of surface to desorb all the impurity for a more precise measure of the m^2/g. The total pore volume (V_{total}) is instead evaluated at a relative pressure P/P^o of 1. According to IUPAC, adsorption isotherms can be classified into six groups.

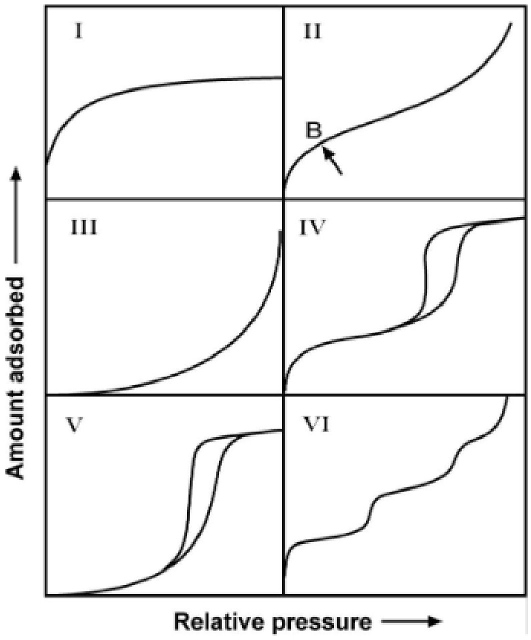

Figure 12 different type of isoterm for N_2 adsorption. Adapted from ("(PDF) Gas Sorption System Operating Manual," n.d.)

Type I isotherms are characteristic of microporous solids with a relatively small external grain surface. Type II isotherms are characteristic of multilayer adsorption and are characteristic of non-porous or macroporous solids. Type III isotherms are characteristic of macroporous solids and are distinguished by having weak adsorption forces, which do not serve to determine the specific area. Type IV and V isotherms correspond to Type II and III when there are mesopores. Finally, type VI isotherms represent layer-by-layer adsorption. ("Gas Sorption System Operating Manual," n.d.)

The first step is the charging of the liquid nitrogen's tank to collect impurity condenses, cleaning the surface consists in collect in a glass test tube a little amount of catalyst and applying a depression (vacuum condition) and heat, in this way it is able to favour the physics and chemical desorption of the impurity, the species will go out from the test glass, they are going to be collected and condensed, thanks to another glass tank immerged in liquid nitrogen.

After depuration it is ready to fill another tank of liquid nitrogen in order to reach the temperature at which nitrogen is going to condense and adsorb on the catalyst's surface. Once filled the test glass with cleaned catalyst, it is connected to the machine, the nitrogen will flow insides and the condensation temperature will be reached thanks to liquid nitrogen tank having the glass test inside it.

The N_2 adsorption analyses were performed on the Quantachrome Autosorb iQ apparatus. Prior to adsorption, samples were degassed under vacuum conditions (110 °C for 7 h). The total pore volume (V_{total}) was determined from the volume of N_2 adsorbed for the relative pressure $P/P^0 = 0.97$, and the BET method was used to determine the specific surface area of activated carbons and catalysts.

3.2.2 TGA

This type of measurement is a thermal analysis method and consists of heating a sample from room temperature to a desired temperature depending on what you want to research. The sample will lose a certain fraction of weight depending on the temperature because there are components present on that sample that decompose or burn (if in the presence of oxygen) at that specific temperature (Russo, 2022).

Samples of ~7 mg for all catalysts and activated carbons were subjected to this analysis. Three types of TGA experiments were carried out. Activated carbons were analysed under N_2 and air flow from room temperature to 900 °C (rate of 10 ºC/min), to evaluate their stability under those atmospheres and, in case of air experiments, quantify the amount of ashes. In addition, all samples were analysed after being their surfaces saturated in water with the aim of testing their hydrophobicity. For these studies, relevant considering that water presents an inhibitory role in the reaction, water desorption was followed from room temperature to 400 ºC (rate of 10 ºC/min). The hydrophobicity was afterwards quantified by calculation of the h index (values ranging from 0 to 1), defined as the ratio between the mass losses corresponding to water weakly interacting with the samples (150 ºC) and all water present in the samples (~400 ºC).

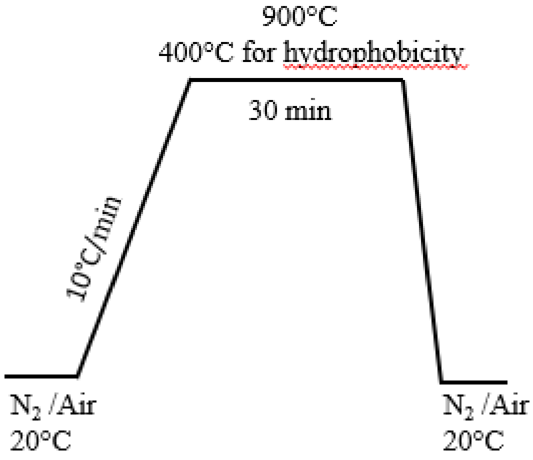

Figure 13 Temperature programme for TGA experiments.

3.2.3 TPR

With temperature-programmed reduction, many components can be studied, including catalysts with metal oxides, zeolites, etc. To study precisely the oxidising species in the sample, a stream of reducing gas, H_2 or CO, mixed with N_2 or He must be flowing in the sample in order to detect the difference in conductivity due to the change in temperature, precisely because a species within the catalyst is reacting. Initially having a flow of hydrogen and argon in the stream, as soon as the hydrogen reduces some component of the catalyst, the temperature will change and the TCD (thermal conductivity detector) will register the difference in electrical conductivity, signalling a peak in the measurement, meaning the consumption of hydrogen; so that the analysis is not compromised, the gas, before passing through the TCD, is let to flow through a trap using solid CO_2 (-200°C), so that all species that come out of the reaction such as water and other compounds are blocked and do not interfere with the measurement.. The TPR concerns the energy aspect of the catalyst, in fact it identifies at what temperature the metal phase inside it is active (Pirola et al., 2018).

In this work, catalysts were pre-treated under 25 mL min^{-1} of Argon flow at 250 °C (metal-containing carbons) or 500 ºC (activated carbon supports), with a ramp of 10 °C/min or 5 ºC/min, respectively, and after this process cooled down at room temperature to start the TPR analysis. Then, from room temperature, TPR analysis was started with a 30 mL min^{-1} flow of 5%H_2/Ar flow and a ramp of 10 °C/min until 500 °C.

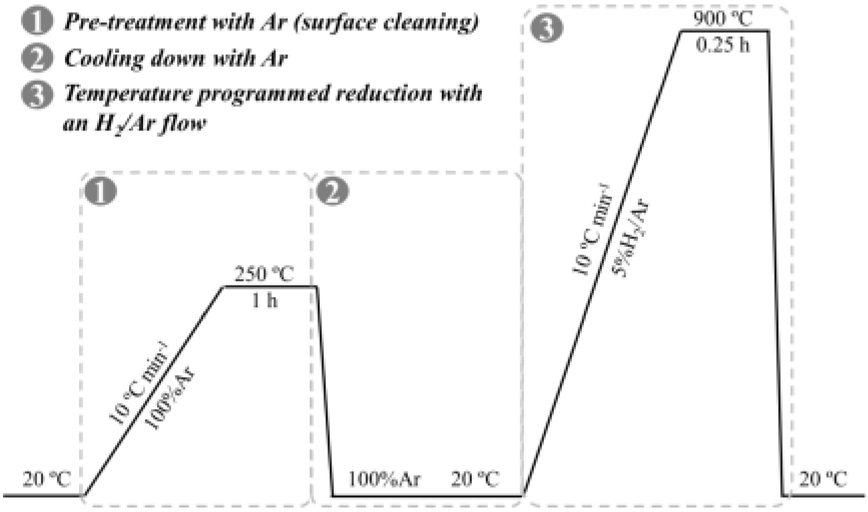

Figure 14 H_2 TPR procedure.

3.2.4 SEM

Scanning electron microscopy (SEM) is a technique that allows the morphology of materials to be analysed with Figures on the order of µm. SEM uses a high-energy electron beam that generates a variety of signals on the surface of the sample. These generated signals derive from the interactions between the electrons and the sample, revealing information about the internal morphology, i.e. its texture, chemical composition, crystal structure and orientation of the crystalline compounds that make up the sample (Sun et al., 2019) .

In this work, activated carbons were analysed by SEM to characterise the shape and size of the internal structure. These analyses were carried out at the Electron Microscopy Laboratory (Microlab) of the Instituto Superior Técnico using a JOEL brand microscope, model 7001. Prior to analysis, the samples were coated with a thin film containing Au-Pd to improve their electronic conductivity and consequently improve the quality of the Figures obtained.

3.2.5 TEM

Transmission electron microscopy (TEM) is an electron microscopy technique that allows the determination of the average size of Ni^o crystallites, as well as the visualisation of metal centres in the media. In this technique, a high-intensity electron beam strikes the sample and the transmitted and diffracted electrons are collected, forming an Figure. In supported catalysts, a sharp contrast can be observed between the metal and the support. To perform the analysis, the samples must be very thin and placed in a vacuum (Russo, 2022).

In this work, TEM analysis was performed for reduced catalysts at the electron microscopy laboratory (Microlab) at the Instituto Superior Técnico using a Hitachi 8100 microscope.

3.2.6 XRD

X-ray diffraction allows the nature and chemical structure of compounds in a sample to be analysed. This technique is based on the principle that when a crystalline solid is subjected to X-rays, the periodically spaced layers of atoms function as a diffraction grating, as an electromagnetic wave enters the crystal lattice and excites the electrons of an atom. which emits radiation of the same wavelength but in a different direction. The intensity of the diffracted X-rays depends on the nature, number and relative position of the atoms in the elementary lattice, but also on the size of the crystallites. The relative position of the peaks in the diffractogram together with the distribution of the relative intensities makes it possible to identify the crystalline material.

X-ray diffraction uses monochromatic radiation of wavelength λ falling on the sample. The sample consists of a large number of crystallites whose orientation is random, with a certain number of crystallites being in the Bragg position for a given set of crystallographic planes h k l (Miller index), i.e. for a given incidence θ, such that Bragg's law is satisfied, as can be seen in the equation

$$n\lambda = 2d_{hkl}\, sin\theta \tag{8}$$

Where θ represents the Bragg angle, d the distance between the interlattice planes and n the integer number of wavelengths.

In this thesis, XRD patterns of fresh and spent catalysts were collected using a Bruker AXS Advance D8 diffractometer equipped with a 1D detector (SSD 160) and using a Ni filter. The scanning range was set from 20 to 80° (2θ), with a step size of 0.03° and a step time of 0.5 s.

3.3 Catalytic tests

3.3.1 Operative conditions

Catalytic tests were conducted in a fixed-bed pyrex reactor with a porous support in the middle, placed in an electric vertical oven from Termolab, being the reaction temperature measured by a thermocouple inserted in the catalyst bed. The inlet flows to the reactor were composed of hydrogen, carbon dioxide and nitrogen. The reactor mixture, diluted with a constant flow of nitrogen, was analysed using Edinburgh Sensors' Guardian® NG detectors for CO, CO_2 and CH_4 (range of 0-10 vol%). In addition to these detectors, a CO_x detector (Ultramat 23 from Siemens) with a sensitivity range of 0 to 1 % (v/v) for both CO and CO_2 was used. This detector is necessary because CO selectivity is generally low, and can reduce the accuracy of values read in the detector with a wider range, i.e. 0 to 10 % (v/v). Furthermore, prior to adding dilution, the reactor flow passes through a 3-way valve, which allows the determination of the flow for each of the reaction temperatures studied. This flow measurement is crucial, since there is a variation in the number of moles in the methanation reaction.

The operating conditions are such that there is a reactor flow rate of 287 mL min^{-1} and a ratio of hydrogen to carbon dioxide of 4:1, so that the stoichiometric reaction is carried out and the three gases H_2, CO_2, N_2, are injected at a molar ratio of 36:9:10 to ensure these conditions. In all tests, 200 mg of catalyst were used to form a very thin layer on the substrate. Each test was preceded by a further reduction under current of nitrogen and hydrogen respectively percentage of 20% and 80%, from room temperature, with a ramp of 5 °C/min, to 470 ºC (1 h) to guarantee the presence of all nickel species in metallic form (active sites for the methanation reaction).

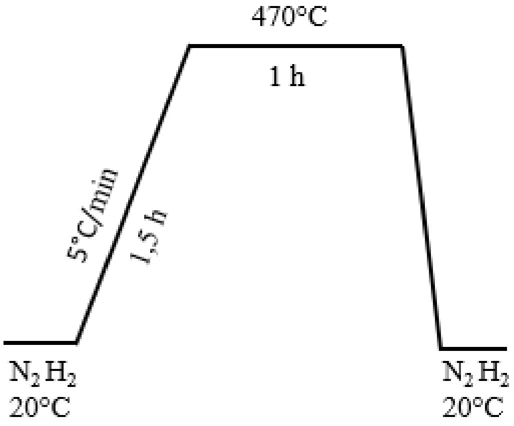

Figure 15 temperature programme for the reduction process

In order to measure the performance of the catalysts in terms of carbon dioxide conversion and selectivity towards methane, a step temperature increase was followed from ~250 to ~450 ºC (Figure 16). For each step, the outlet flow and composition were measured under steady-state conditions.

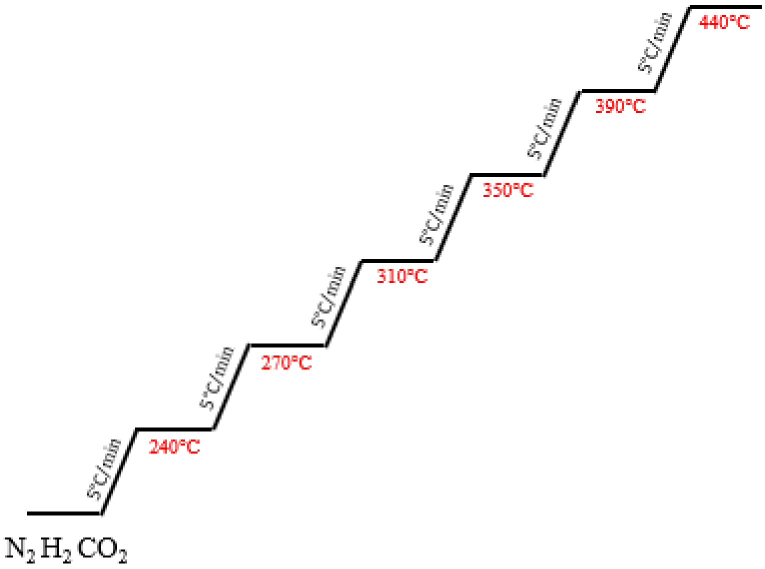

Figure 16 Temperature programme for catalytic tests measurements.

3.3.2 Determination of CO_2 conversion and CH_4 selectivity

The carbon dioxide conversion was calculated by considering the difference between the molar inflow and molar outflow divided by the molar inflow, all multiplied by 100.

$$CO_2\ conversion\ (\%) = \frac{FCO_{2\,in} - FCO_{2\,out}}{FCO_{2\,in}} \times 100 \tag{9}$$

Due to the fact that selectivity towards a specific product is given by the ratio of the molar flow rate of the product divided by the difference between the inlet and outlet molar flows of the limiting reagent, we can define the two following selectivities:

$$CH_4\, selectivity\ (\%) = \frac{FCH_{4\, out}}{FCO_{2\, in} - FCO_{2\, out}} \times 100$$

(10)

$$CO\ selectivity\ (\%) = \frac{FCO_{out}}{FCO_{2\, in} - FCO_{2\, out}} \times 100$$

(11)

Where F denotes the molar flow rate and since we are in low pressure conditions (atmospheric pressure), it can be calculated via the perfect gas equation

$$PV = nRT \quad ; \; n = \frac{PV}{RT}$$

(12)

$$F = \frac{PQ}{RT}$$

(13)

Finally, methane yields were obtained as follows:

$$CH_4\ yeld = \frac{conv\ CO_2(\%) \times select\ CH_4(\%)}{100}$$

(14)

Having given the definition of all these measurements, in reality to be able to arrive at a result and thus calculate conversion, selectivity and yield, one would first have to know what the volume flow rate is at the reactor outlet. The first thing to consider is the flow rate of diluted nitrogen (355 mL). In addition, to know the volumetric fluxes of the components at the reactor outlet, it is sufficient to multiply the volumetric flux at the reactor outlet by the concentration of the given component, given by the detector:

$$Q_{Detectors} = Q_{out\ Reactor} + Q_{dilution} = Q_{out\ Reactor} + 355$$

(15)

$$QCO_{2\ out} = Q_{out\ Reactor} \times C(CO_{2\ Detector})$$

(16)

$$QCO_{\ out} = Q_{out\ Reactor} \times C(CO_{\ Detector})$$

(17)

$$QCH_{4\ out} = Q_{out\ Reactor} \times C(CH_{4\ Detector})$$

(18)

4. *Results and discussion*

4.1 Activated carbons characterization

As already described, activated carbons were derived from coconut shell waste being activated through chemical and physical processes. Activated carbons were firstly characterized by SEM analysis, being the results presented in Figure 17, Figure 18 and Figure 19 for AC_H, AC_Z and AC_C, respectively.

Starting by AC_H results (Figure 17), some contaminants are identified. Namely, phosphorus peaks were the most intense, with traces of iron, nickel, chromium and titanium also present, probably from the activation process. The structure of the coal results without a defined shape.

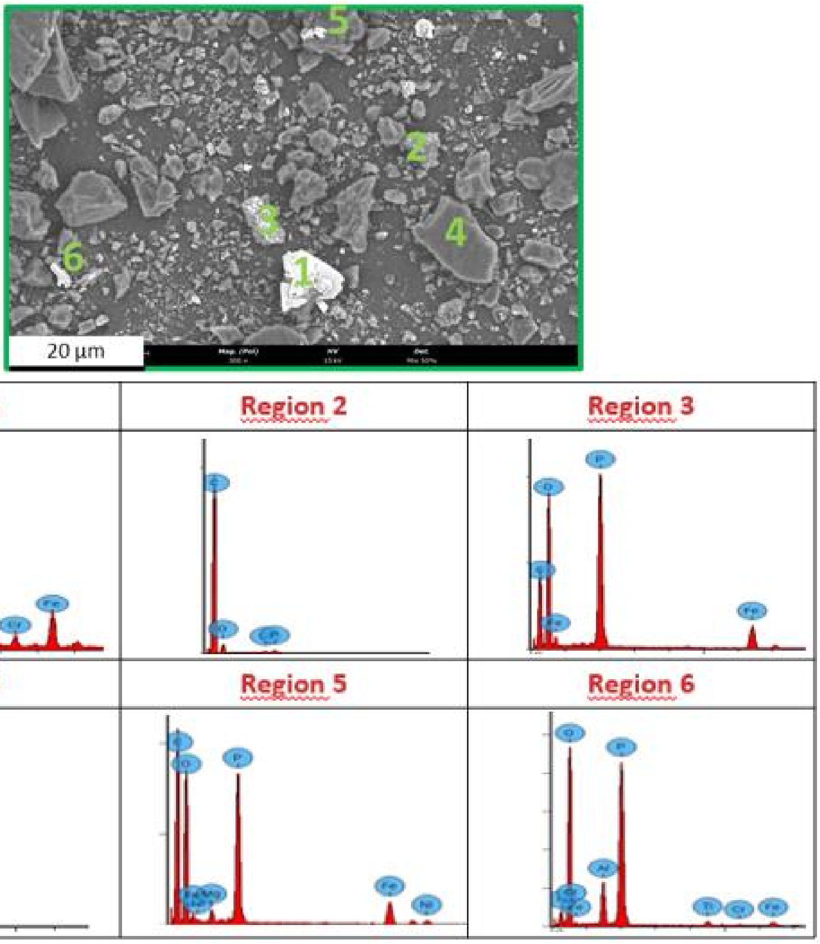

Figure 17 SEM results for AC_H with a scale of 20 micron and EPS.

In the case of AC_Z (Figure 18), the presence of zinc and chlorine was detected, probably resulting from the activation process were $ZnCl_2$ was use as chemical agent. As far as shape is concerned, a hexagonal structure can be observed here.

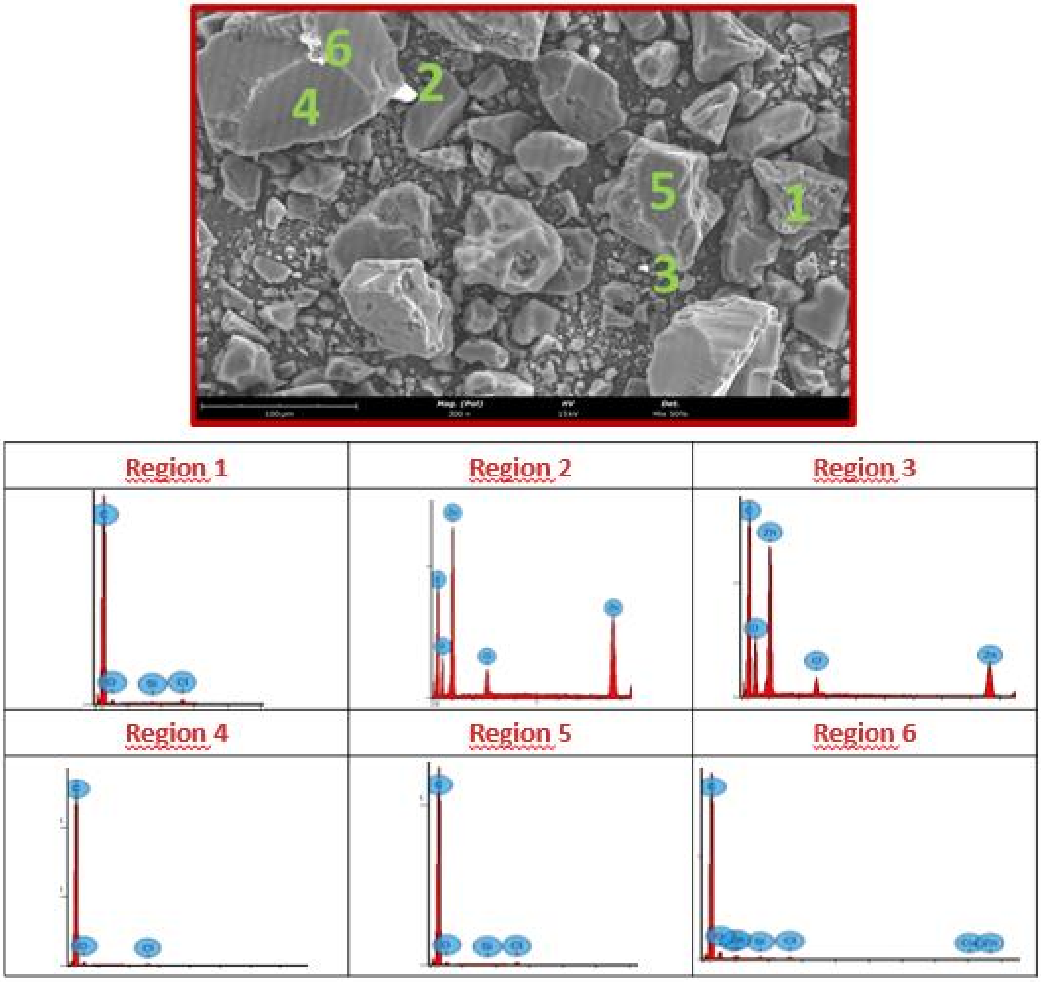

Figure 18 SEM results for ACz with a scale of 100 micron and EPS.

With regard to AC_C (Figure 19), the catalyst activated by physical methods, i.e. with carbon dioxide and at high temperature and without external chemical compounds, it can be noted that only contaminants that are part of the molecular structure of the coconut are present. In fact, mainly potassium, silicon, sodium and aluminium were found, which are constituents of the coconut biomass.

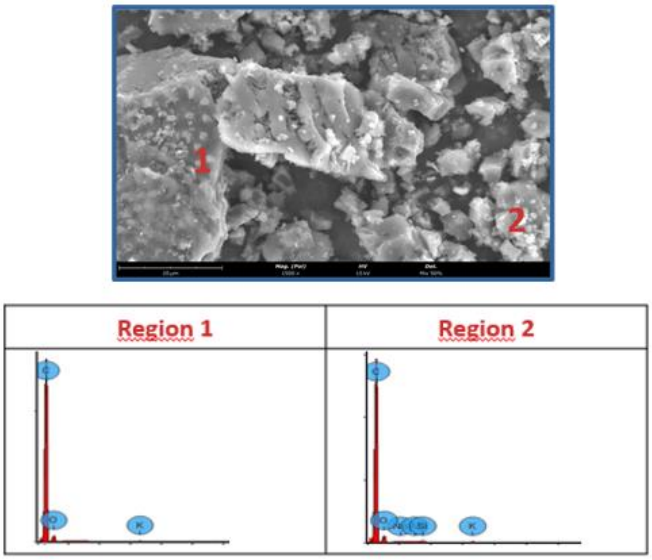

Figure 19 SEM results for ACc with a scale of 20 micron and EPS.

Thermal gravimetric analyses were also performed under a nitrogen atmosphere to assess the thermal stability of the materials (Figure 20). Results indicate that ACz and ACc are stable up to 500 °C, while AC_H up to 400 °C. Also, a mass loss in the initial part of the analysis, around 150 °C, showed a loss of water in all samples. Around 600 °C, the mass loss for AC_H and AC_C begins to increase dramatically until, by the end of the analysis, a mass loss of the material of ~95% is reached. This indicates that only the metallic contaminants of the material remain. Indeed, as seen before in SEM images (Figure 17), the presence of iron, chromium, nickel, titanium and phosphorus was detected for AC_H, while K, Si, Na and Al were found in AC_C. These are not able to decompose like carbon, as their melting temperature is well above 800 °C ("Punti di Fusione dei Metalli | La Terra e il Fuoco," n.d.). As far as AC_Z is concerned, at the end of the whole process there will only be a 20 % loss of mass.

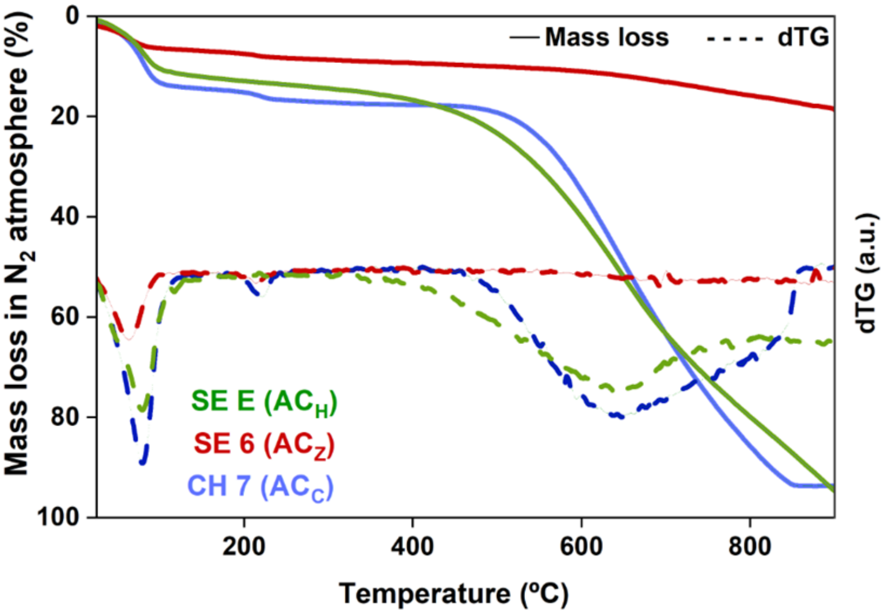

Figure 20 TGA results for activated carbons analysed from room temperature until 900 °C under nitrogen flow. Continuous lines refer to mass losses and discontinuous ones to dTG results.

It was also intended to evaluate by means of TGA how the three carbons behaved, in terms of weight loss, with air as the analysis gas (Figure 21 and Figure 22). In addition, trends from the analysis performed under nitrogen were added to compare the results in Figure 21. Due to the fact that the carbon burns due to the oxygen in the air at 550 to 700 °C ("Carbon | Facts, Uses, & Properties | Britannica," 2022), there is a significant and earlier loss of mass than with nitrogen, more or less at the same temperature for all carbons due to oxidation reaction of the carbon at around 550 °C. As already mentioned, activated charcoal does not achieve 100 % weight loss, since inorganic contaminants are present. The fact that AC_H starts to decompose as early as 400 °C could lead during the catalysts' calcination step at 500 °C to an actual percentage of nickel on the catalyst higher than the nominal. Furthermore, as it can be seen by following the dotted lines in Figure 22, at around 500-600°C isothermal decomposition takes place. Due to the fact that the carbon is starting to burn and release heat, it is possible to note that the energy giving of the machine for the sample, between 500°C and 650°C, starts to decrease.

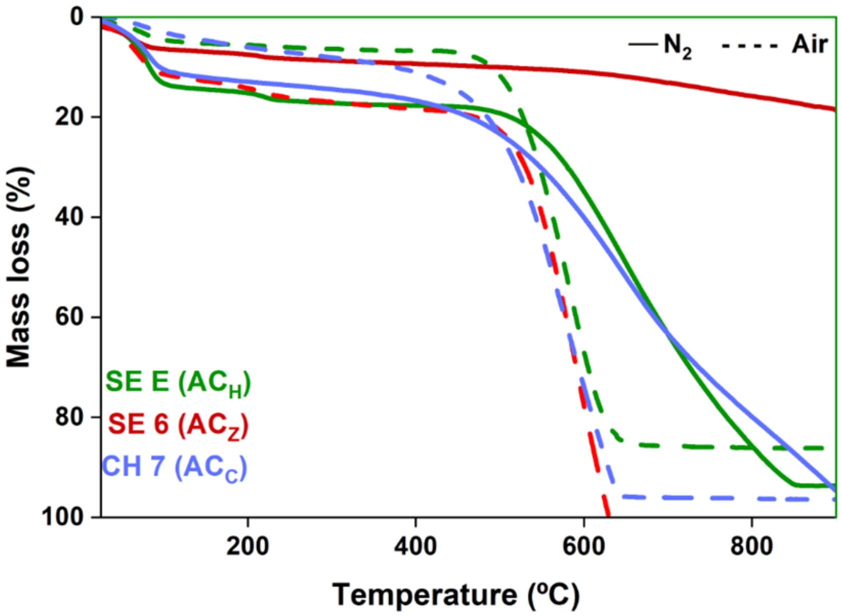

Figure 21 TGA results for activated carbons analysed from room temperature until 900 ºC under both nitrogen (straight line) and air (dotted line) flows.

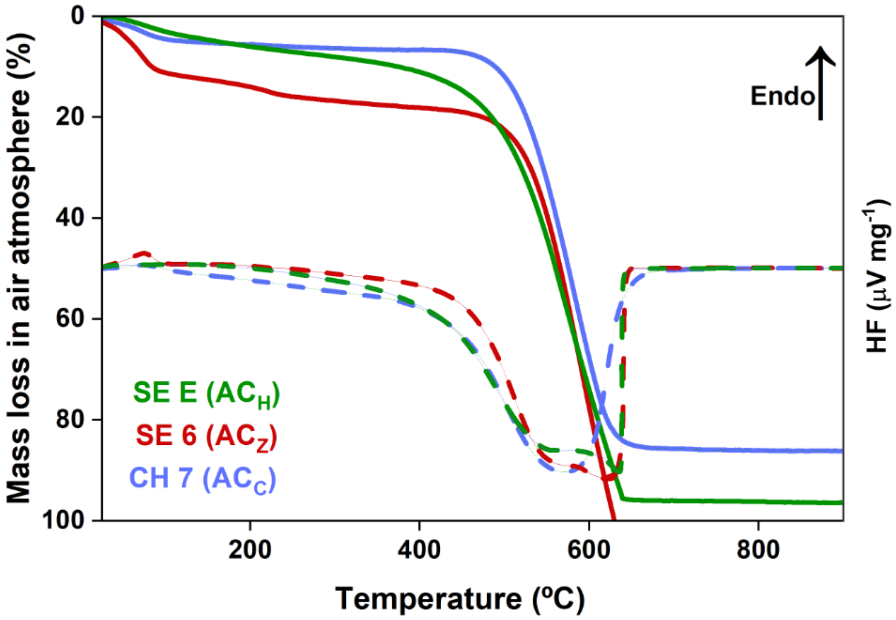

Figure 22 TGA results for activated carbons analysed from room temperature until 900 ºC under air flow. Straight lines refer to mass losses and dotted ones to heat flow results.

As far as XRD analysis is concerned (Figure 23), it can be seen that the broad band at 20 to 35º area is attributed to the amorphous structure of the material (Omri and Benzina, 2012). Also, there are peaks attributed to contaminants in the activated carbon. For instance, the diffraction peaks located at 31.61°, 34.26°, 36.10°, 47.37°, 56.40°, 62.68° and 67.72° correspond to the (100), (002), (101), (102), (110), (103), and (112) reflection planes of hexagonal structure of ZnO for ACz, the one treated with $ZnCl_2$ (Pelicano et al., 2017).

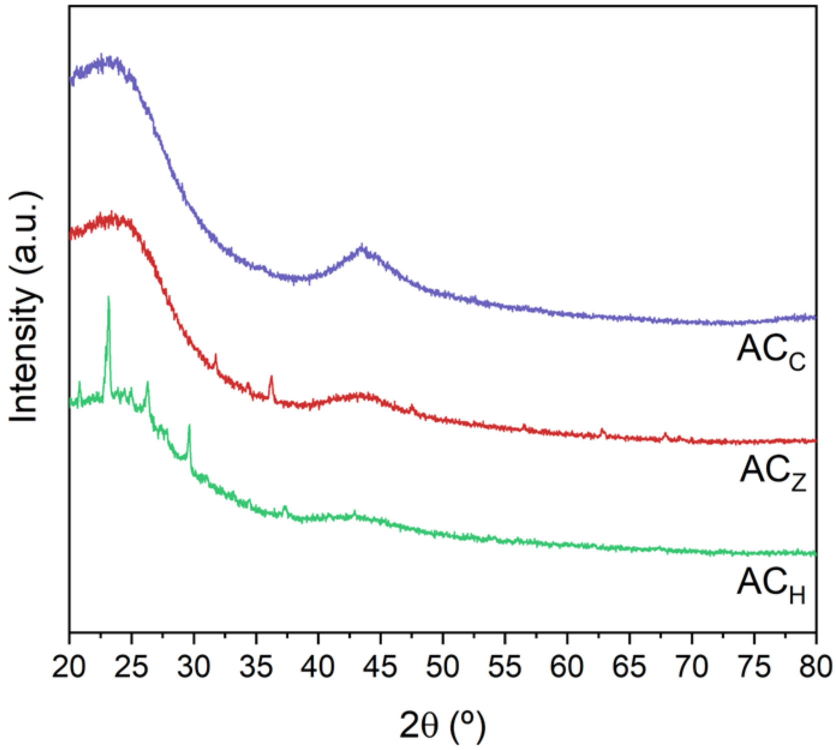

Figure 23 Diffractograms of the three different activated carbons.

Regarding nitrogen adsorption results, presented in Figure 24 and Figure 25, AC_H and AC_Z presented higher textural properties than AC_C both in terms of pore volumes and BET surface area. Indeed, it was possible to identify the trends of Langmuir isotherms in Figure 24, i.e. of microporous materials, pronounced and confirmed in the case of ACc where a higher V_{micro} fraction can be seen than in macropores. As far as AC_H and AC_Z are concerned, it is possible to associate their isotherms with the type IV and V isotherms relating to mesopores, as these have a higher percentage of mesopores than micropores. Furthermore, during desorption there is hysteresis, which undoubtedly confirms the presence of mesopores. These results do not reflect other N_2 adsorption analyses concerning activated carbons derived from coconut shells as those presented in this thesis are far superior to, for example, those presented by (Gao et al., 2018). On the other hand, as far as other supports are concerned, the results of this work higher than those obtained for gamma-alumina in literature (Abate et al., 2016). Finally, from the analysis of the pore size distribution by BJH method (Figure 25), one can confirm that the three activated carbons present mostly micropores.

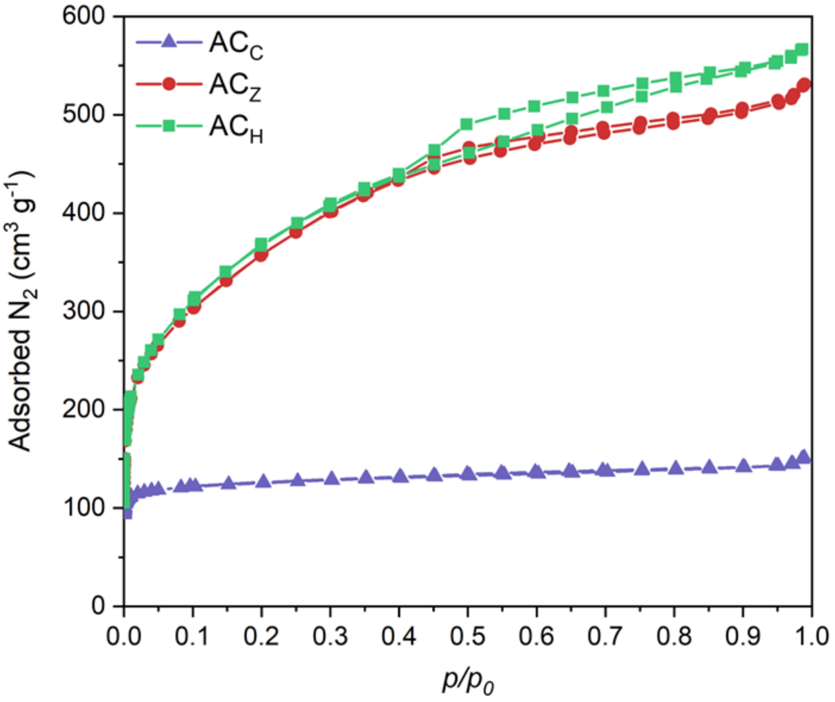

Figure 24 N_2 isotherms of the three activated carbons

Table 4.1 Textural properties obtained by N_2 adsorption and pHpzc (provided by FCT NOVA) for the three activated carbons.

Support	**V_{micro} (cm^3/g)**	**V_{meso} (cm^3/g)**	**A_{BET} (m^2/g)**	**pHpzc**
AC_C	**0.16**	**0.06**	**473**	**9,7**
AC_Z	**0.10**	**0.70**	**1246**	**6,2**
AC_H	**0.14**	**0.73**	**1285**	**2,4**

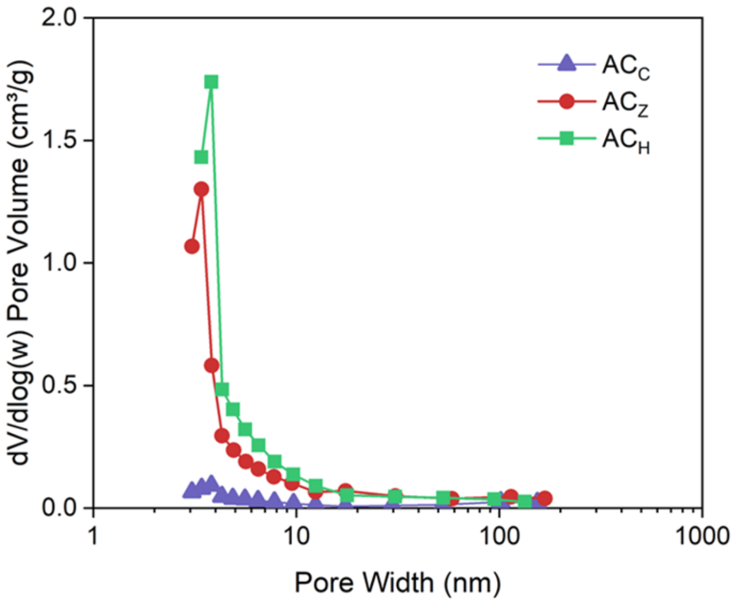

Figure 25 Pore size distribution obtained for the three activated carbons by BJH method.

Finally, pHpzc values were provided by FCT NOVA and presented in Table 4.1. This parameter indicates the acidic-basic properties of the support, an important parameter for CO_2 methanation reaction. As observed, the basicity, favorable property for carbon dioxide activation, followed the order: $AC_C > AC_Z > AC_H$.

4.2 Nickel catalysts

4.2.1 Characterization

Considering the N_2 sorption results and as already indicated in the experimental section of this thesis, the activated carbon presenting the best textural properties to effectively disperse metal particles (AC_H) was chosen to optimize the Ni loading. For this purpose, Ni contents from 2 to 30 wt.% were tested. Besides this, 20 wt.% Ni catalysts were also prepared supported over AC_C and AC_Z activated carbons.

N_2 adsorption isotherms for these series of catalysts are presented in Figure 26 and Table 4.2, being verified that the volume of the mesopores and the specific surface areas generally decrease when the amount of nickel increases. These results are expected since increasing the amount of loading inevitably leads to the presence of the particles in the surface and in the pores of the carbon. To be pointed out is the increase of the specific surface area for $2Ni/AC_H$, $20Ni/AC_C$ and $20Ni/AC_Z$ when comparing to their supports. In these cases, it is suggested that the calcination at 500 ºC performed for decomposing nickel nitrate indued also an opening of the carbons' pores by partial decomposition of the materials, increasing its specific surface area.

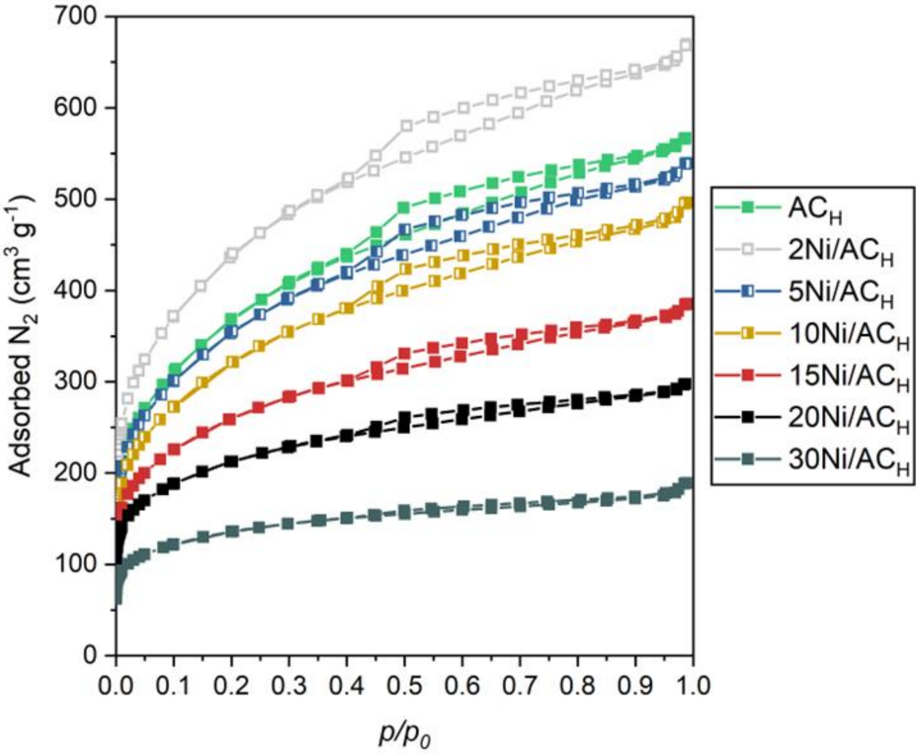

Figure 26 N_2 isotherms for different Ni loading on AC_H

Table 4.2 Textural properties of nickel loading on different activated carbons

Catalyst	**V_{micro} (cm^3/g)**	**V_{meso} (cm^3/g)**	**A_{BET} (m^2/g)**
AC_H	**0.14**	**0.73**	**1285**
$2Ni/AC_H$	**0.17**	**0.84**	**1532**
$5Ni/AC_H$	**0.15**	**0.66**	**1239**
$10Ni/AC_H$	**0.14**	**0.60**	**1124**
$15Ni/AC_H$	**0.15**	**0.43**	**922**
$20Ni/AC_H$	**0.16**	**0.29**	**763**
$30Ni/AC_H$	**0.12**	**0.16**	**493**
AC_Z	**0.10**	**0.70**	**1246**
$20Ni/AC_Z$	**0.14**	**0.40**	**902**
AC_C	**0.16**	**0.06**	**473**
$20Ni/AC_C$	**0.19**	**0.06**	**531**

From the pore size distribution presented in Figure 27 it can be also seen that all AC_H catalysts contain micropores, being their extent reduced with increasing Ni contents. This could be due to nickel particles blocking.

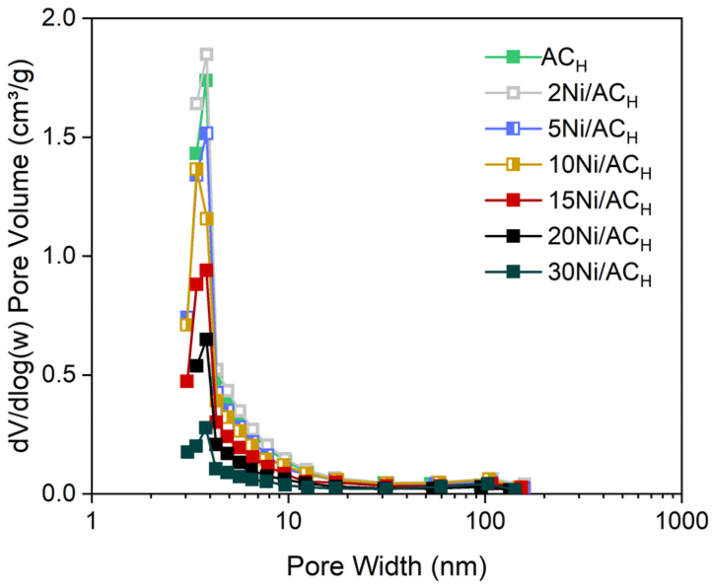

Figure 27 Volume of pores as function of pores' dimensions (nm)

It was also intended to assess whether the nickel nitrate was decomposed during heat treatment, and in fact, it can be seen from Figure 28 that there is already a mass loss of 80% at around 350 °C. To correlate the bonding of nickel nitrate with the activated carbon, the mass loss corresponding to the 15Ni/AC$_H$ catalyst not subjected to calcination was also evaluated (85% around 500 °C). The three trends of the analysis were then correlated regarding the non-calcined 15Ni/AC$_H$ catalyst, the AC$_H$ base and the nickel nitrate used to impregnate the catalyst. So comparing these three materials, it can be seen that the nickel nitrate is almost completely decomposed at 350 °C, while the activated carbon (AC$_H$) shows a decrease in weight but not as much relevant at that temperature (350 °C), which means that the mass loss found in the uncalcined 15Ni/AC$_H$ (85% at 500 °C) catalyst is attributed entirely or almost entirely to the decomposition of the nickel nitrate. This confirms that, after calcination at 500 °C, no nickel nitrate is expected to remain in the materials.

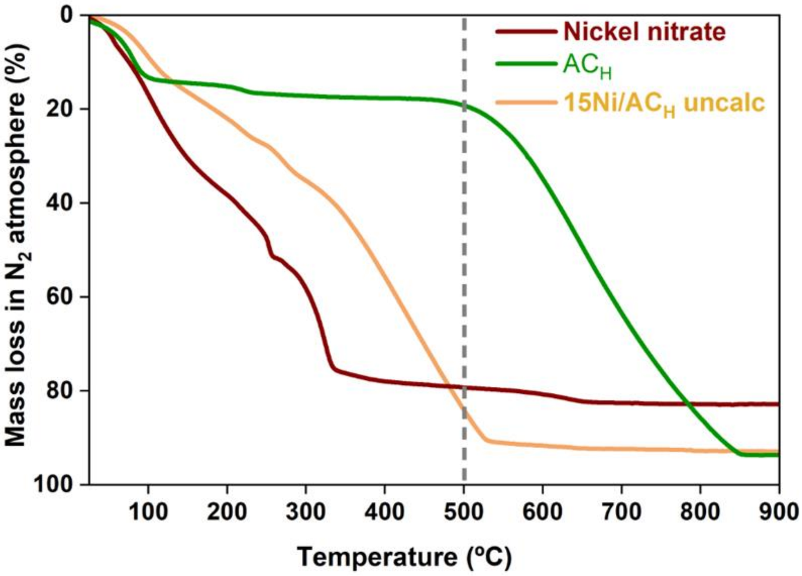

Figure 28 TGA of AC$_H$, nickel nitrate and 15Ni/AC$_H$

In accordance with (Jovic et al., 2006), diffraction peaks for metallic Ni (Ni^0) were found in the Ni catalysts at around 45°,53°, 78° (Figure 29), proofing that the carbons were able to reduce nickel even during the thermal treatment under inert atmosphere (nitrogen).

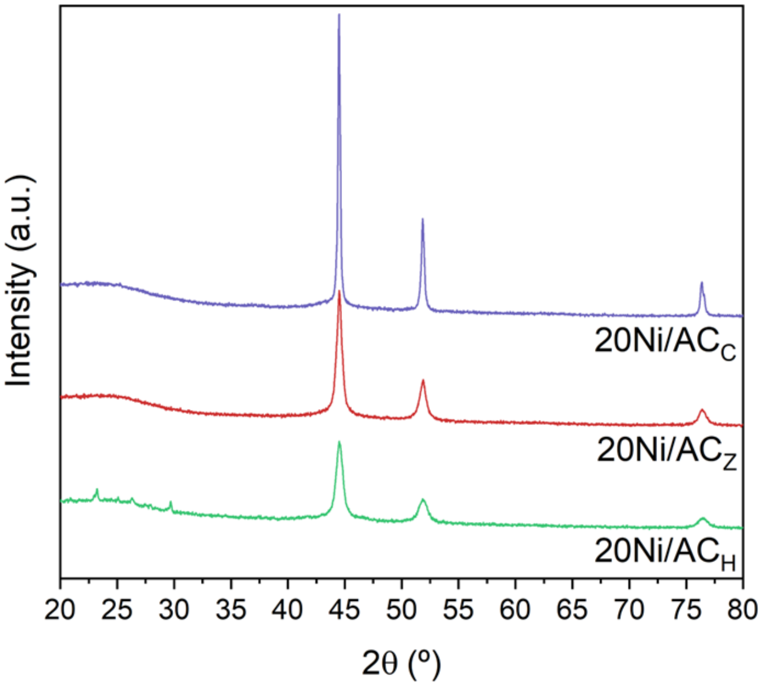

Figure 29 Diffractogram of 20Ni/ACc, 20Ni/ACz, 20Ni/ACH, fresh condition

Regarding H_2-TPR, the variations of the TCD signal can be due to the consumption of H_2 due to metal oxides reduction or the release of other compounds from the carbon supports. According to XRD results previously discussed, the presence of NiO in the catalysts was not detected. However, H_2-TPR results exhibited in Figure 30 and Figure 31 present TCD signal variations below 500 ºC. Indeed, while the peaks below 350 ºC could be ascribed to a very thin layer of nickel oxides formed on the surface of the metallic nickel clusters during the contact with air, peaks at higher temperatures could be ascribed to a partial decomposition of the activated carbons under hydrogen atmosphere, in accordance with the profiles obtained for AC_H, AC_Z and AC_C without addition of metals.

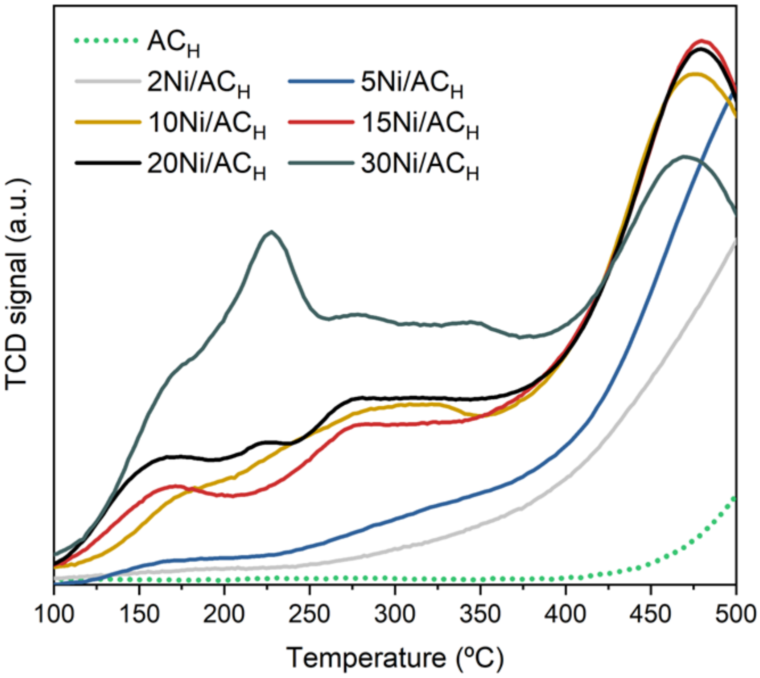

Figure 30 TPR showing TCD signal as function of temperature for different nickel loading

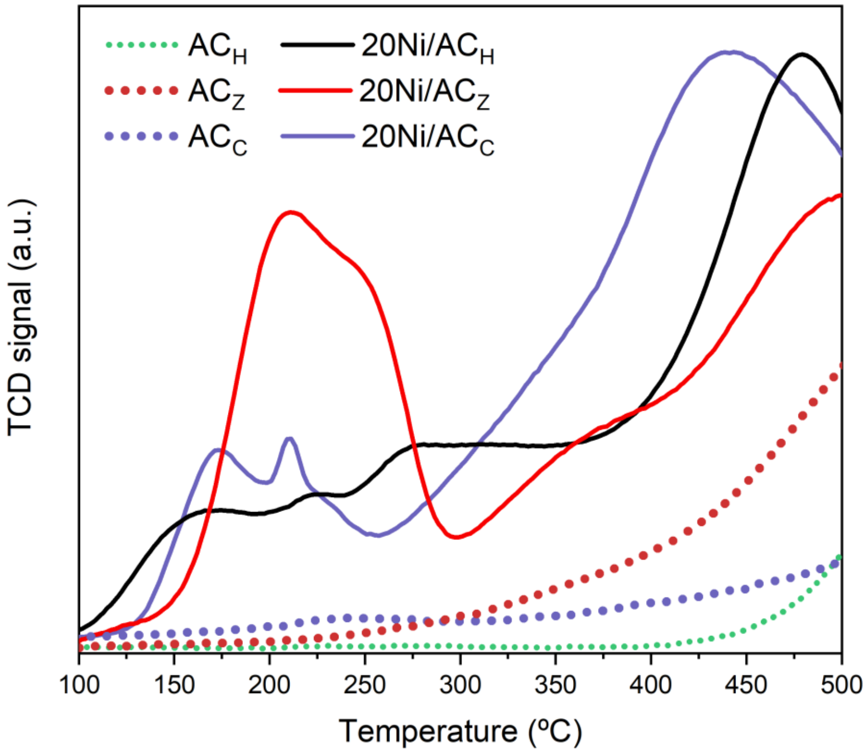

Figure 31 comparisons with TPR of 20Ni/activated carbons and TPR activated carbons

In terms of TEM results, in the next Figure 32 it is possible to see that the surface of the activated carbons is generally homogeneous and with absence of clear particles.

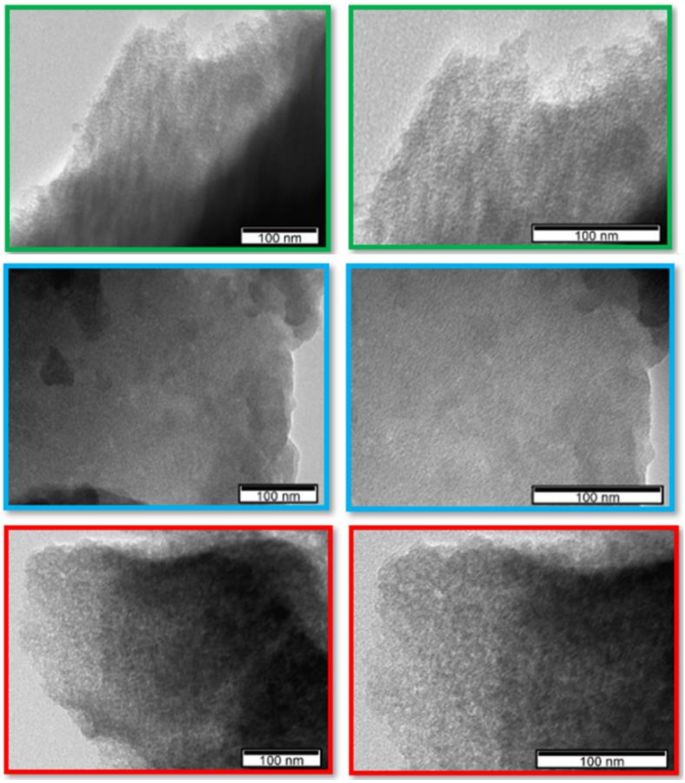

Figure 32 TEM micrographs with a scale of 100 nanometres for AC$_H$, ACc and ACz respectively

In addition, regarding the different Ni loadings over AC_H, it can be clearly seen from the TEM results in Figure 33,Figure 34,Figure 35 and Figure 36 that larger particles are formed for higher metal contents. This effect could thus explain the reduction of the textural properties with the increase of Ni wt.%.

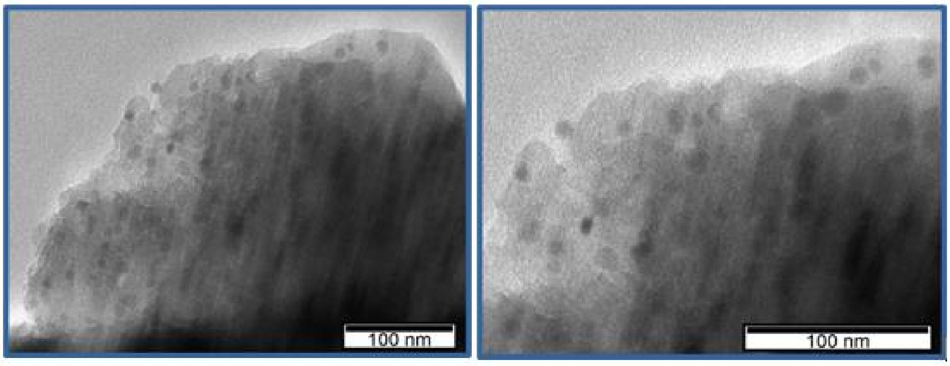

Figure 33 TEM migrographs with a scale of 100 nanometres for 5%Ni/AC_H.

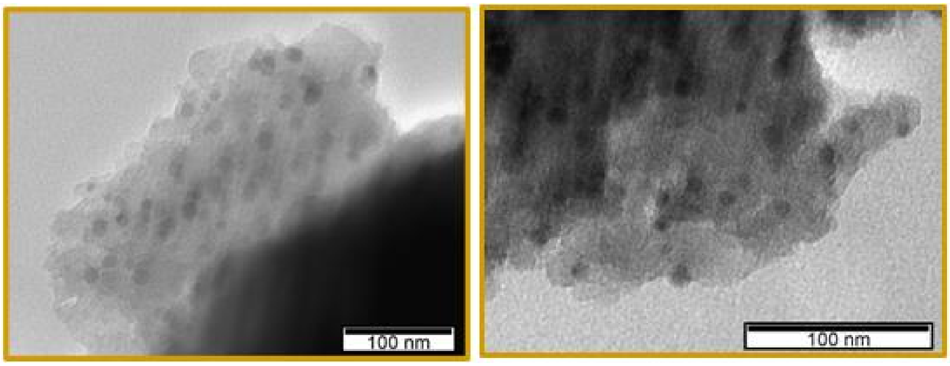

Figure 34 TEM migrographs with a scale of 100 nanometres for 10%Ni/AC_H.

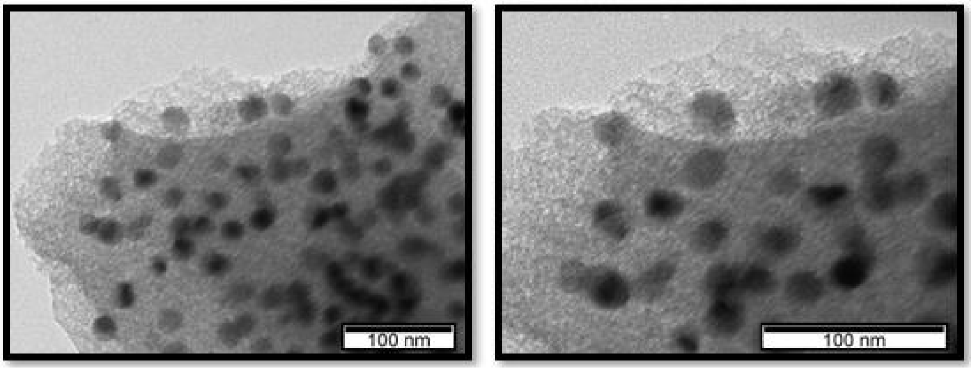

Figure 35 TEM migrographs with a scale of 100 nanometres for 20%Ni/AC_H.

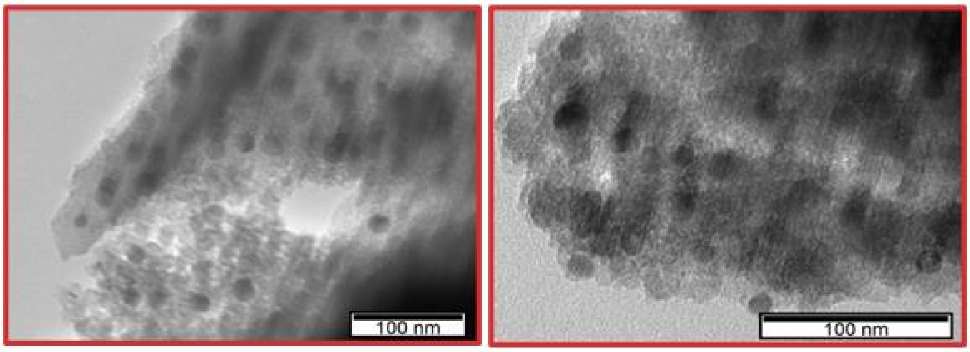

Figure 36 TEM migrographs with a scale of 100 nanometres for 30%Ni/ACH.

In terms of the type of activated carbon influence in the metal particles size, the comparison of TEM results from Figure 36 (20Ni/ACH), Figure 37 (20Ni/ACC), and Figure 38 (20Ni/ACZ) suggest that all materials allow a homogeneous dispersion of the nickel metal particles.

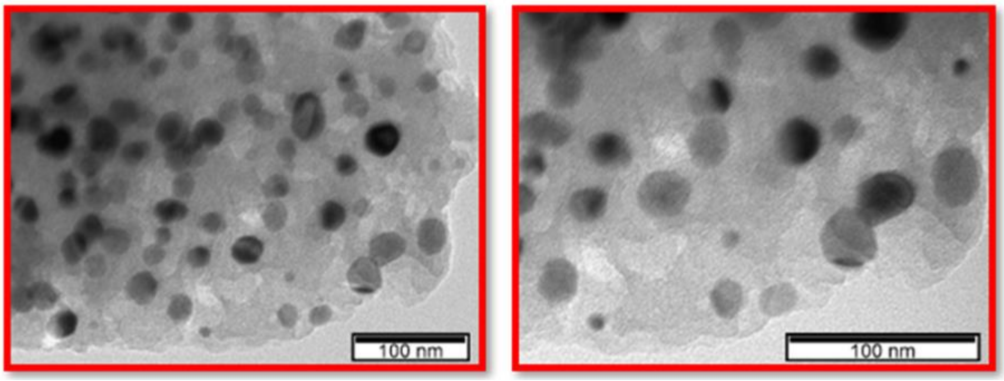

Figure 37 TEM migrographs with a scale of 100 nanometres for 20%Ni/ACc.

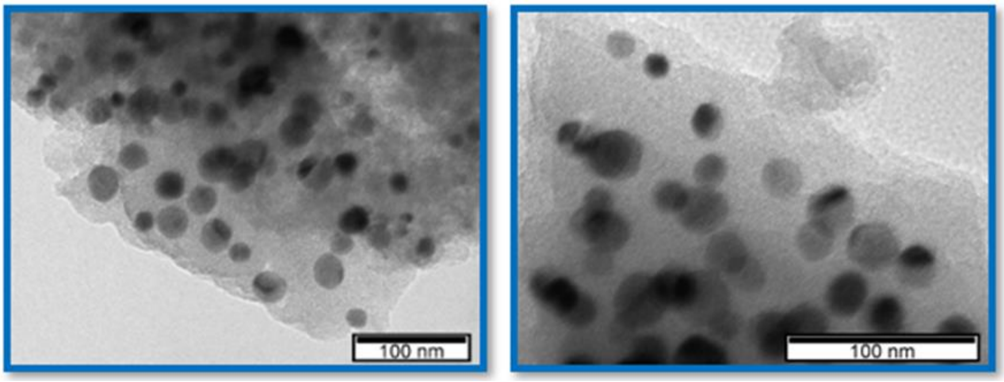

Figure 38 TEM migrographs with a scale of 100 nanometres for 20%Ni/ACz.

By analysing TEM micrographs, average Ni^0 particle sizes and dispersions were determined (Table 4.3), being the histograms presented in Figure 39 and Figure 40. As observed, the increase of the particle sizes with the Ni loading was confirmed. In addition, regarding 20 wt.% Ni catalysts, the smallest Ni^0 particles and, consequently, highest metallic dispersion was obtained for 20Ni/ACC. The gaussians shape obtained for the histograms also suggests that the particles were homogeneously distributed in terms of size in all the supports.

Table 4.3 Average Ni^0 particle sizes and metallic dispersions for Ni catalysts.

Catalyst	**ØNi^0 (nm)**	**Dispersion (%)**
5Ni/AC$_H$	10	8
10Ni/AC$_H$	12	7
20Ni/AC$_H$	21	4
30Ni/AC$_H$	17	5
20Ni/AC$_Z$	24	4
20Ni/AC$_C$	16	5

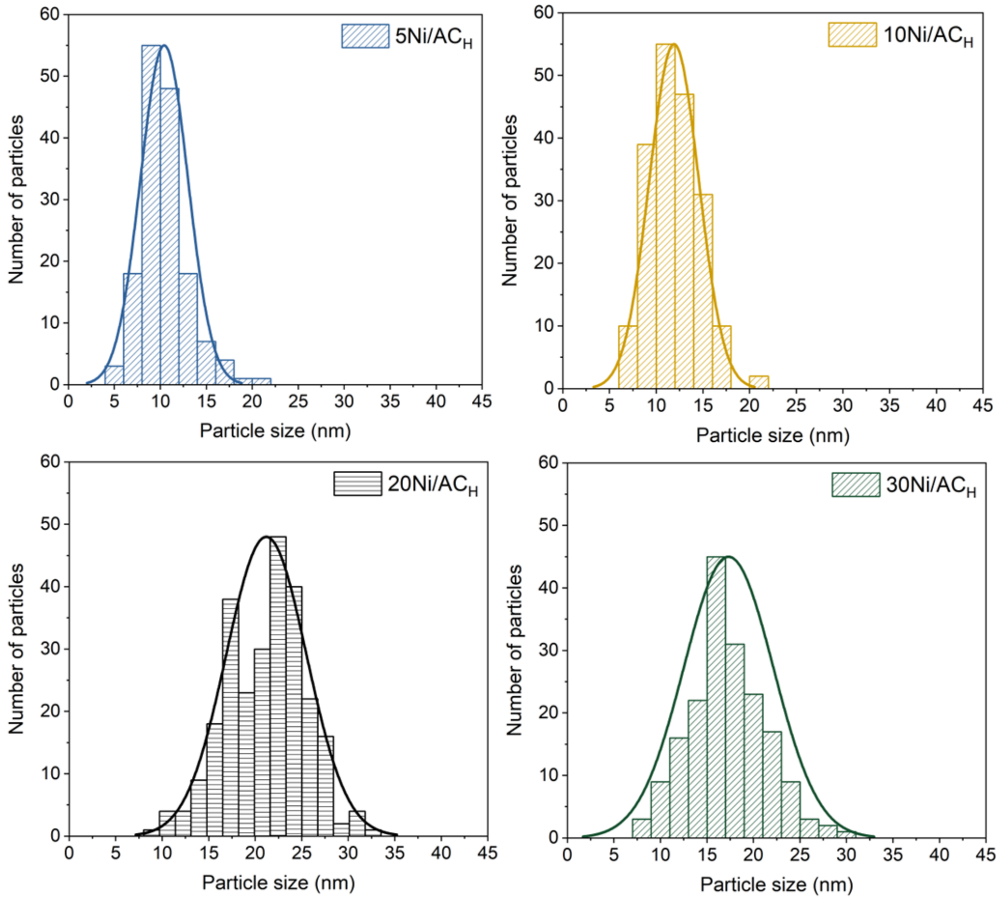

Figure 39 Particle size distribution, number of particle as function of size(nm) of different loading on AC$_H$

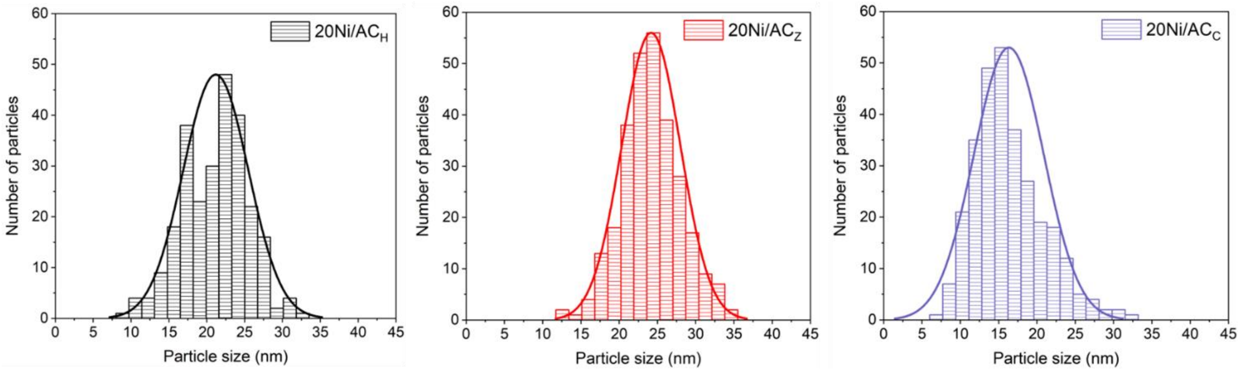

Figure 40 Particle size distribution, number of particle as function of size(nm) of 20Ni on three carbons

4.2.2 Catalytic test for Nickel catalysts

Catalysts based on AC_H and containing variable Ni loading were firstly tested, being the best performances presented in Table 4.4. As observed, none of the materials exhibited activities higher than 5 %. These results were ascribed to a poisoning effect of the impurities found in the activated carbon support. Taking this into account, and in accordance with literature studies where Ni loadings were optimized for other type of porous supports such as zeolites, a content of 20 wt.% Ni was chosen as the more favourable.

Table 4.4 Best catalytic performances obtained for AC_H-supported catalysts with variable Ni loadings.

Catalyst	**Best performances**		
	T (ºC)	**Conversion (%)**	**Selectivity (%)**
2Ni/AC_H	**446**	**2**	**89**
5Ni/AC_H	**447**	**1**	**44**
10Ni/AC_H	**452**	**2**	**<1**
15Ni/AC_H	**460**	**4**	**10**
20Ni/AC_H	**448**	**4**	**12**
30Ni/AC_H	**446**	**5**	**51**

Considering the catalysts with 20 wt.% Ni and supported over the three types of activated carbons, the best catalytic performances can be found in Table 4.5. Indeed, the catalyst supported over AC_C presented the best results, in accordance with the higher basicity of this carbon support and the more favourable metallic dispersion. Again, the poorest activity and selectivity was delivered by AC_H carbon catalyst, probably due to the negative impact of the impurities in the properties of the material. Finally, the performances of $20Ni/AC_Z$ were lower than those of the $20Ni/AC_C$ but considerably better than $20Ni/AC_H$. This could be due to the intermediate basicity and metallic dispersion in this sample.

Table 4.5 Best catalytic performances obtained for the 20 wt.% Ni catalysts supported over activated carbons at 450 ℃.

Catalyst	**Best performances**		
	T (ºC)	**Conversion (%)**	**Selectivity (%)**
$20Ni/AC_H$	**448**	**4**	**12**
$20Ni/AC_C$	**448**	**46**	**35**
$20Ni/AC_Z$	**449**	**39**	**28**

Catalysts with 20 wt.% Ni loading were also characterized after test by XRD (Figure 41). It is possible to note that no remarkable reoxidation of nickel is expected during the experiments, as no additional diffraction peaks are observed.

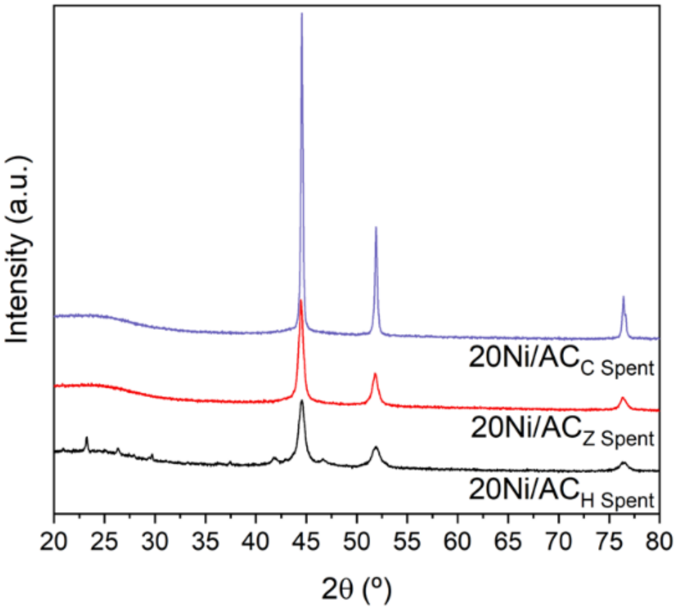

Figure 41 Diffractograms of $20Ni/AC_C$, $20Ni/AC_Z$ and $20Ni/AC_H$ after catalytic tests.

4.3 NiCe catalysts

4.3.1 Characterization of Ni-Ce catalysts

Starting by N_2 sorption results (isotherms in Figure 42 and textural properties in Table 4.6), results indicate that the addition of a second metal leads to a reduction of the surface areas and pore volumes. Again, this could be ascribed to the above-mentioned principle in which the available area decreases because it is occupied by metal clusters.

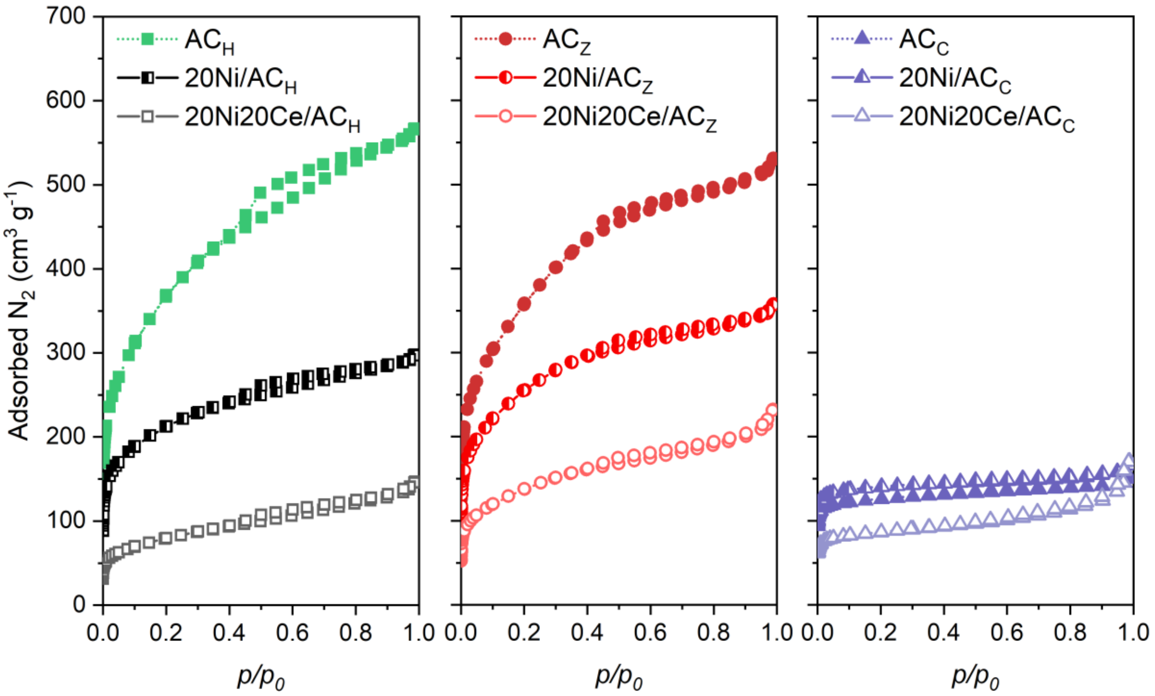

Figure 42 Comparisons of diffent isotherms comparing activated carbon, 20%Ni and 20% Ni 20%Ce

Table 4.6 Textural properties of activated carbons, 20Ni and 20Ni 20Ce on the carbon

Support	**V_{micro} (cm^3/g)**	**V_{meso} (cm^3/g)**	**A_{BET} (m^2/g)**
AC_C	**0.16**	**0.06**	**473**
$20Ni/AC_C$	**0.19**	**0.06**	**531**
$20Ni20Ce/AC_C$	**0.10**	**0.12**	**322**
AC_Z	**0.10**	**0.70**	**1246**
$20Ni/AC_Z$	**0.14**	**0.40**	**902**
$20Ni20Ce/AC_Z$	**0.07**	**0.26**	**487**
AC_H	**0.14**	**0.73**	**1285**
$20Ni/AC_H$	**0.16**	**0.29**	**763**
$20Ni20Ce/AC_H$	**0.04**	**0.17**	**281**

Furthermore, a similar behaviour to monometallic nickel catalysts occurs for doped catalysts in terms of pore sizes distribution determined by BJH method (Figure 43). Indeed, with a second metal an even smaller volume of micropores was found out due to the blockage of the particles, in this case certainly greater due to the presence of the cerium particles.

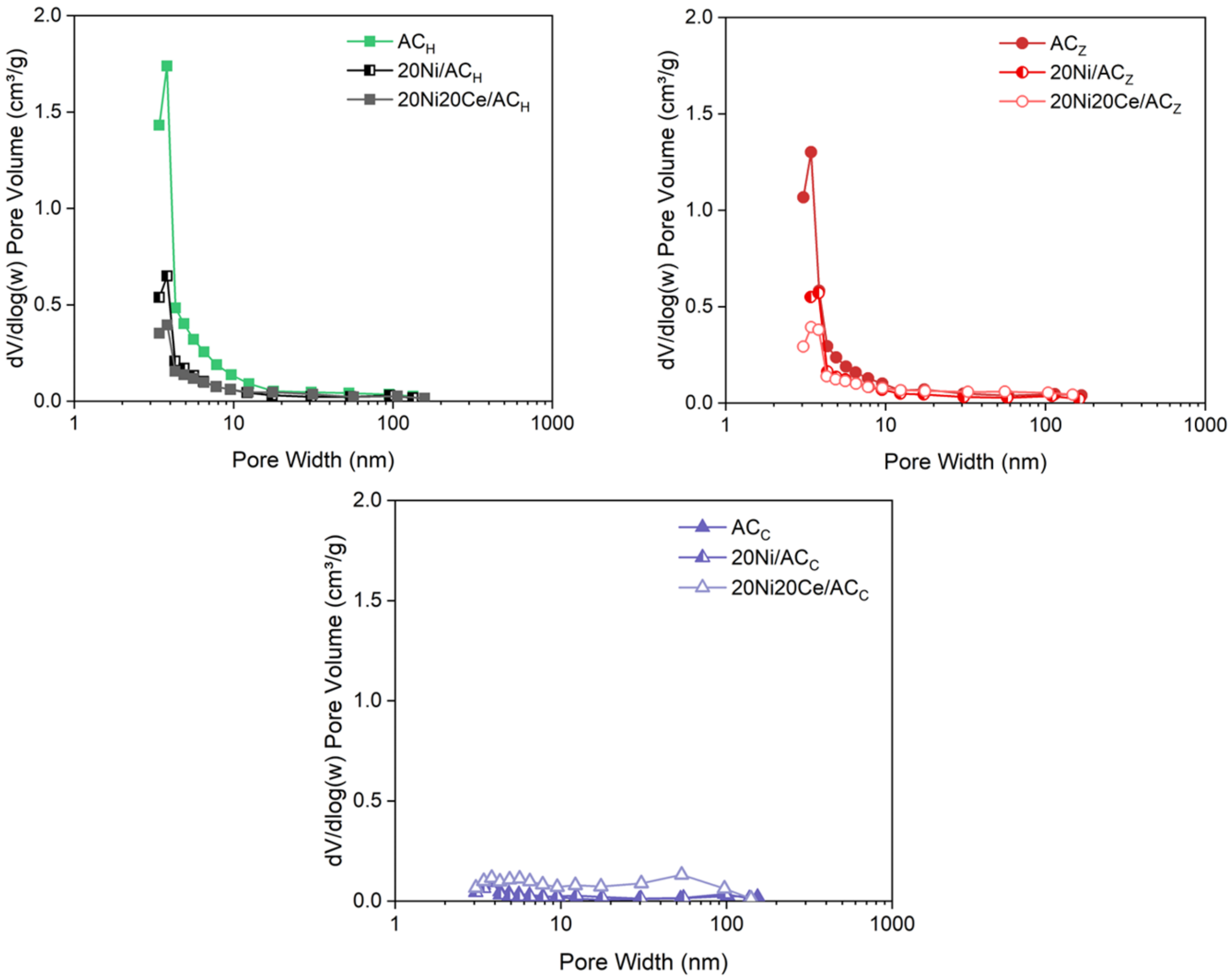

Figure 43 Pore volume as function of pore size

The hydrophobicity of the catalysts (tendency not to retain water inside it or on its surface) was also analysed by calculating h indexes (Table 4.7). It is of fundamental importance to study this property on catalysts in this work, as water is a reaction product. Since water is a reaction product, if it is retained on the surface of the catalyst (low hydrophobicity), the reaction will be shifted towards the reactants with a consequent decrease in conversion. If, on the other hand, the catalyst has a high hydrophobicity, the water tends to leave the surface of the catalyst immediately, enabling the reaction to produce new products immediately and thus shift the reaction to the right. As can be seen from Table 4.7, all h-indexes are close to 1, which indicates that all the catalysts are highly hydrophobic. Thus, the reaction should not be strongly inhibited by the presence of water produced by the reaction.

Table 4.7 h index for 20Ni and 20Ni20Ce on three different activated carbons

Catalyst	**20Ni/AC$_H$**	**20Ni/AC$_C$**	**20Ni/AC$_Z$**	**20Ni20Ce/AC$_H$**	**20Ni20Ce/AC$_C$**	**20Ni20Ce/AC$_Z$**
h index	**0,95**	**0,91**	**0,99**	**0,82**	**1,00**	**0,91**

In terms of XRD patterns for cerium-doped catalysts (Figure 44), ceria peaks were detected at 29°, 33°, 48°, and 56°, in accordance with (Ghanbary and Jafarnejad, 2017) and (Abate et al., 2016). In addition, metallic nickel diffraction peaks were again observed, indicating that nickel was also reduced in these samples.

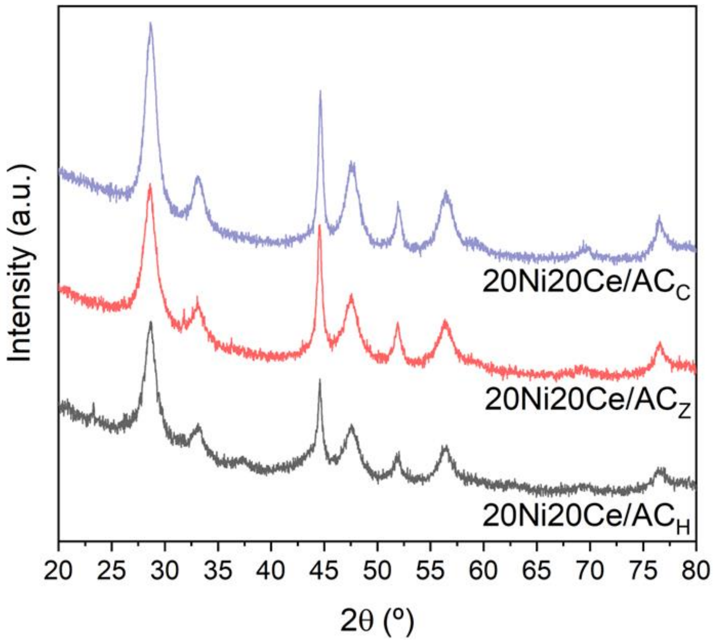

Figure 44 XRD diffractograms of 20Ni20Ce-based catalysts.

Furthermore, and as previously observed for Ni catalysts, TCD signal variations were detected in H_2-TPR experiments (Figure 45 and Figure 46). While reduction processes below 350 ºC could be ascribed to a layer of NiO over the metallic particles due to the contact with the ambient and peaks above 400 ºC could suggest the decomposition of the activated carbon (especially for AC$_Z$), one cannot exclude the reduction of well-dispersed ceria species at ~400 ºC. Indeed, by analysing Figure 46, where Ni and NiCe catalysts are compared to their corresponding activated carbon support, it is clear the presence of more intense peaks in the Ce-containing samples for the three carbons, probably due to the additional reduction of CeO_2 in the temperature range under analysis.

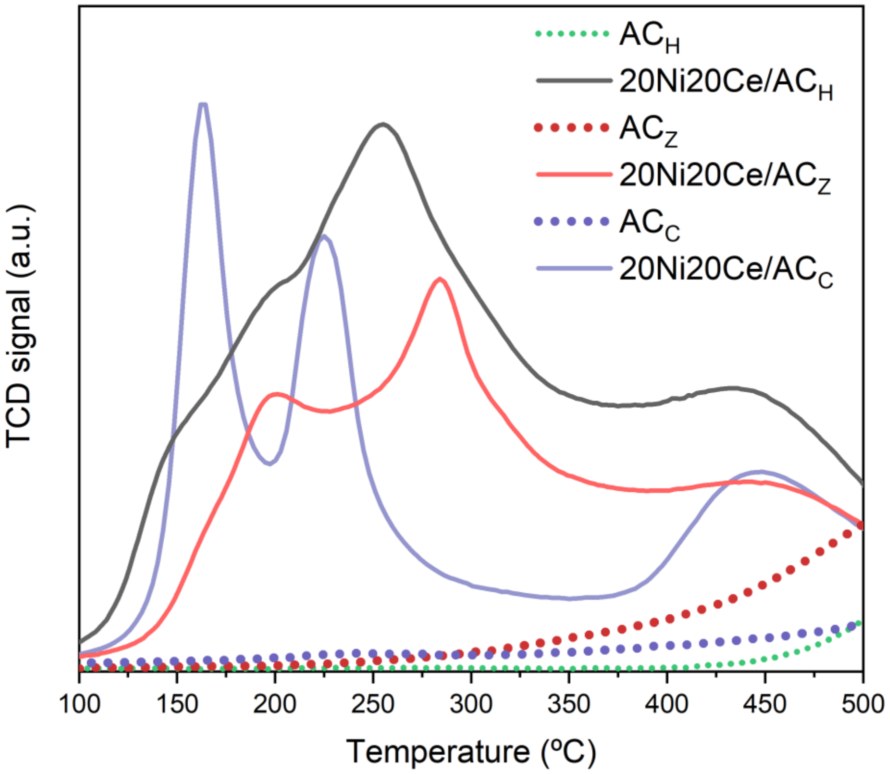

Figure 45 Comparisons between activated carbon and doped catalyst

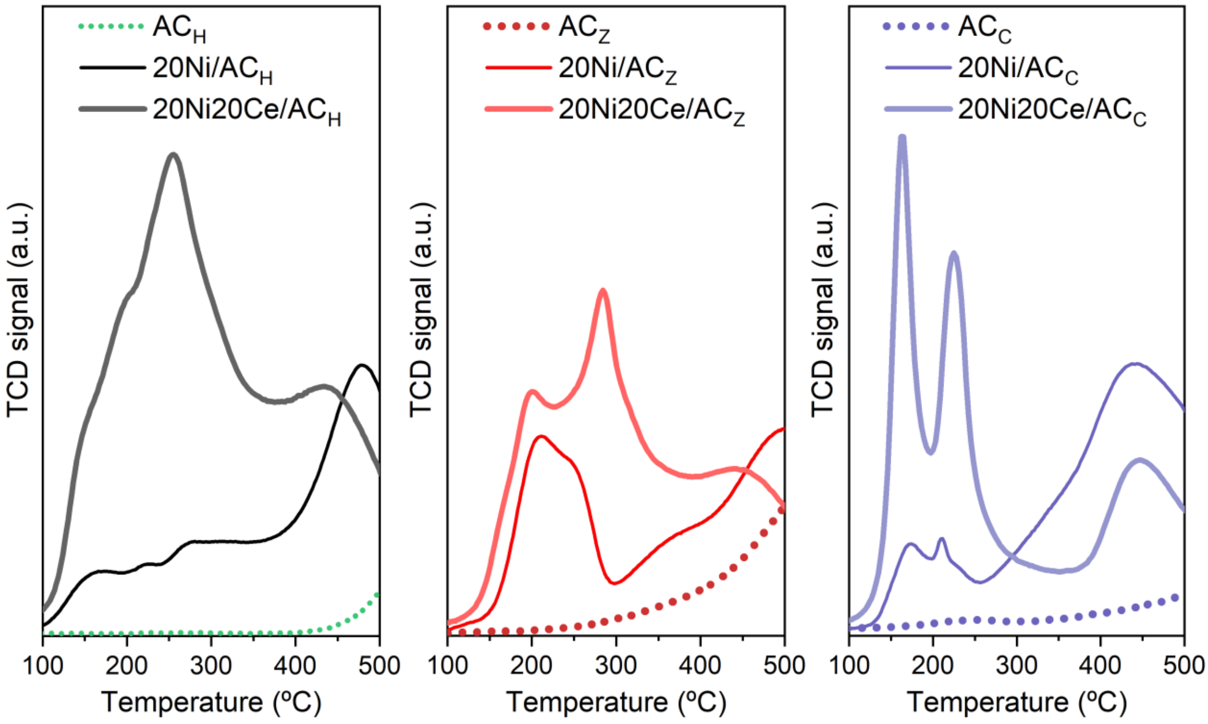

Figure 46 TPR of 20Ni and 20Ni20Ce and its base

As stated by (Bacariza et al., 2018) and (Martin et al., 2019), and in accordance with TEM results presented in Figure 47, Figure 48, Figure 49 and, especially, Figure 47, reduced nickel particles tend to become smaller and better distributed when cerium is introduced.

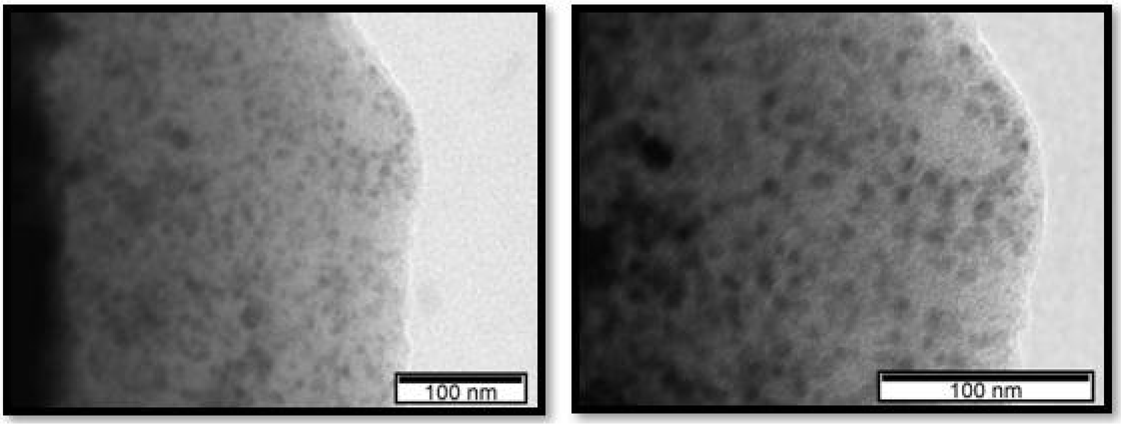

Figure 47 TEM micrograph with a scale of 100 nanometres for 20Ni20Ce/AC$_H$.

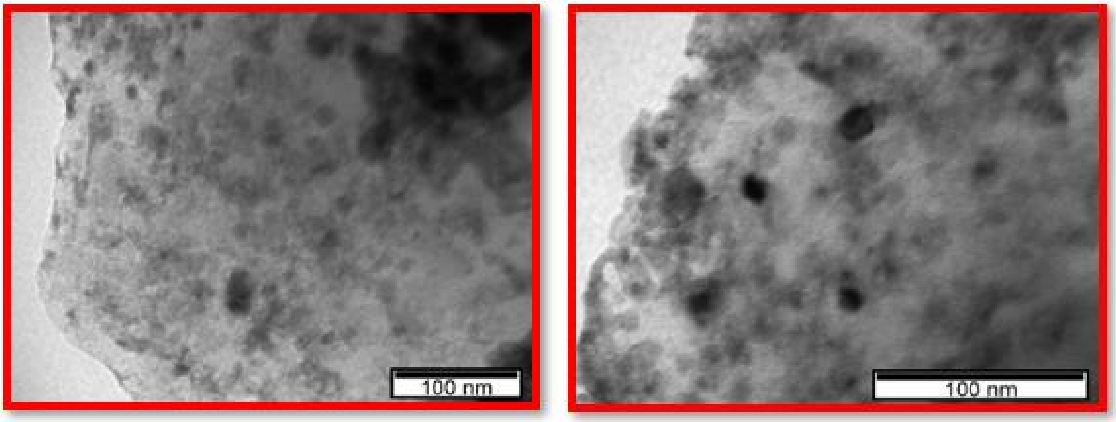

Figure 48 TEM micrograph with a scale of 100 nanometres for 20Ni20Ce/AC$_C$.

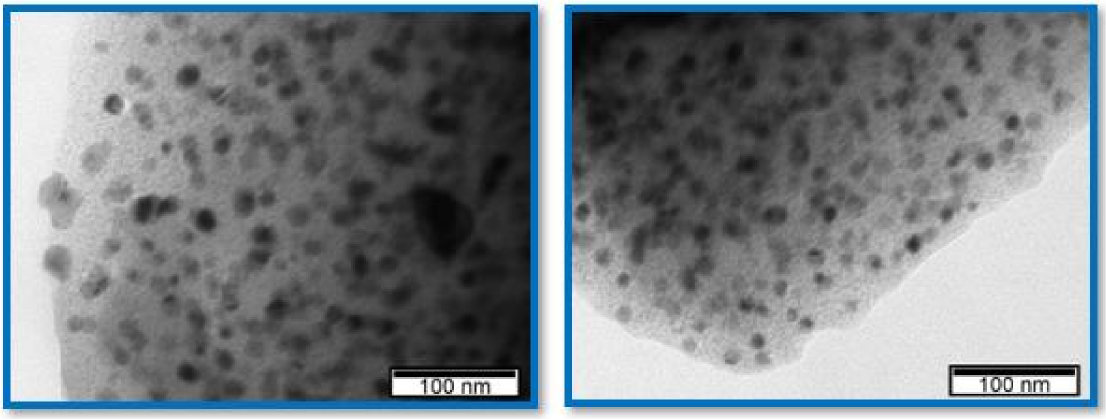

Figure 49 TEM micrograph with a scale of 100 nanometres for 20Ni20Ce/AC$_Z$.

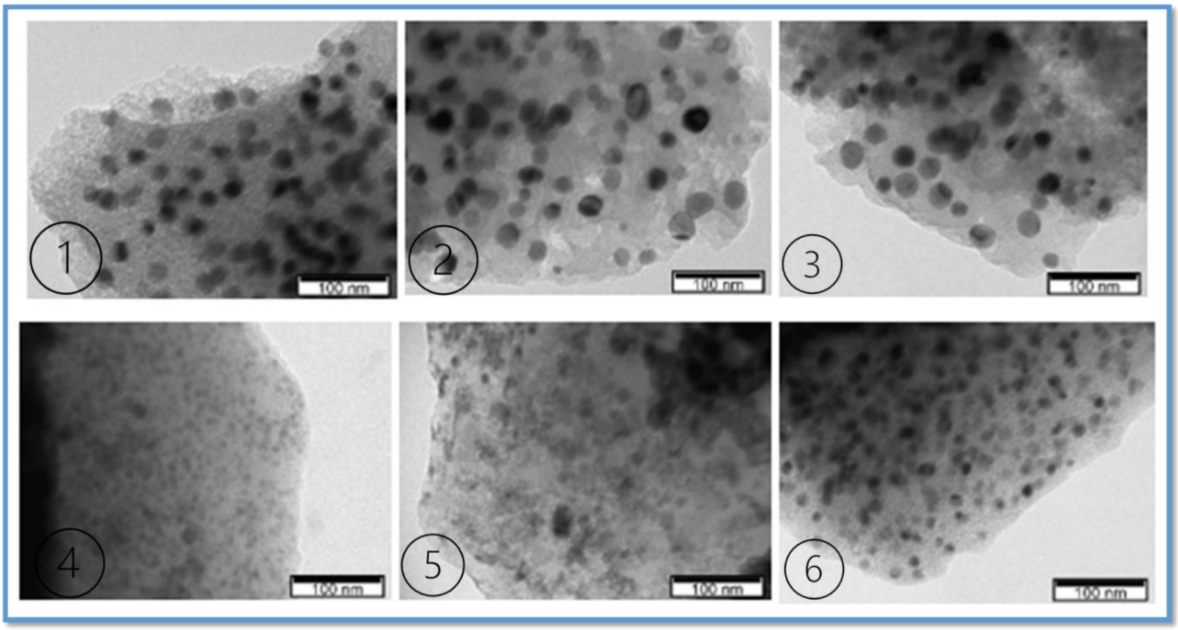

Figure 50 TEM micrographs with a scale of 100 nanometres for: (1) 20Ni/AC$_H$, (2) 20Ni/AC$_C$, (3) 20Ni/AC$_Z$, (4) 20Ni20Ce/AC$_H$, (5) 20Ni20Ce/AC$_C$ and (6) 20Ni20Ce/AC$_Z$.

Based on the analysis of the particle sizes, metallic dispersions and histograms (Table 4.8 and Figure 51), it is confirmed that the addition of Ce reduces the size of Ni^0 particles improving the dispersion. In fact, there was a decrease in nickel particles diameter when comparing NiCe with Ni catalysts corresponding to 66% for 20Ni20Ce/AC$_H$, 46% for 20Ni20Ce/AC$_Z$ and 50% for 20Ni20Ce/AC$_C$. Besides this, it is clearly observed that when comparing cerium and non-cerium catalysts in Figure 51, the histogram tends to shift towards smaller sizes and its amplitude tends to decrease, resulting in a greater number of particles with the same diameter.

Table 4.8 Average diameter of Ni^0particles and metal dispersion for 20Ni and 20Ni20Ce on three different activated carbons

Catalyst	**ØNi^0 (nm)**	**Dispersion (%)**
20Ni/AC$_H$	21	4
20Ni20Ce/AC$_H$	7	13
20Ni/AC$_Z$	24	4
20Ni20Ce/AC$_Z$	13	7
20Ni/AC$_C$	16	5
20Ni20Ce/AC$_C$	8	11

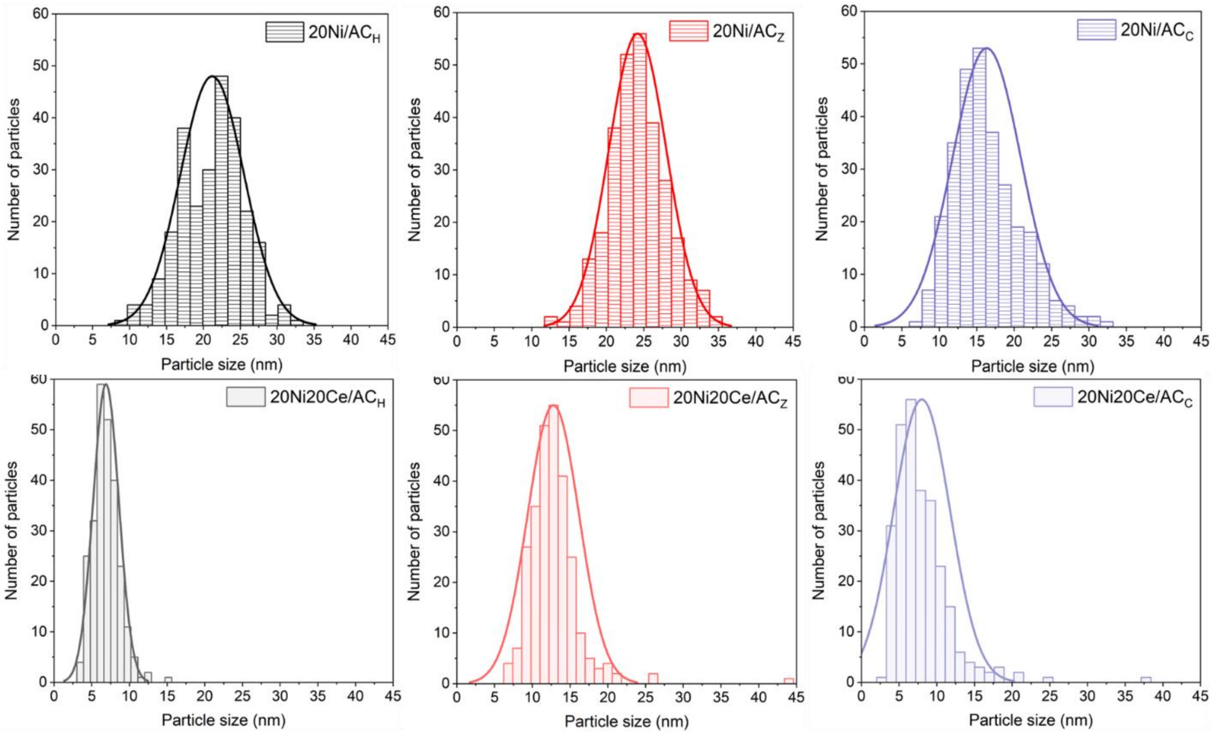

Figure 51 Histograms of the 20Ni- and 20Ni20Ce-based AC_H, AC_z and AC_c catalysts.

4.3.2 Catalytic test for Ni-Ce catalysts and comparisons

The catalytic performances of samples containing 20 wt.% Ni and 20 wt.% Ce as well as the monometallic Ni references can be found in Figure 52. As observed, and due to Ce' ability to reduce the size of metallic nickel particles and efficiently activate CO_2 , (Bacariza et al., 2018) and (Martin et al., 2019), the conversion passed from ~5% for 20Ni/AC_H to ~80% for 20Ni20Ce/AC_H. In fact, although all doped catalysts showed a conversion higher than 70% at ~360 °C, the best doped catalyst was the one supported over the worst activated carbon, with a conversion of 81% at 360 °C. In terms of selectivity to CH_4 (the other by-product being CO in all cases), it is very close to the thermodynamic limit, while in terms of yield, the best catalysts presenting very similar results are NiCe based on AC_H and AC_C. It is interesting to note that methane selectivity drops dramatically with increasing temperature and the absence of cerium in the catalyst, whereas it remains very high and follows the trend of thermodynamics in the case of doped catalysts, confirming and even exceeding the selectivity values obtained by (Fujita and Takezawa, 1997).

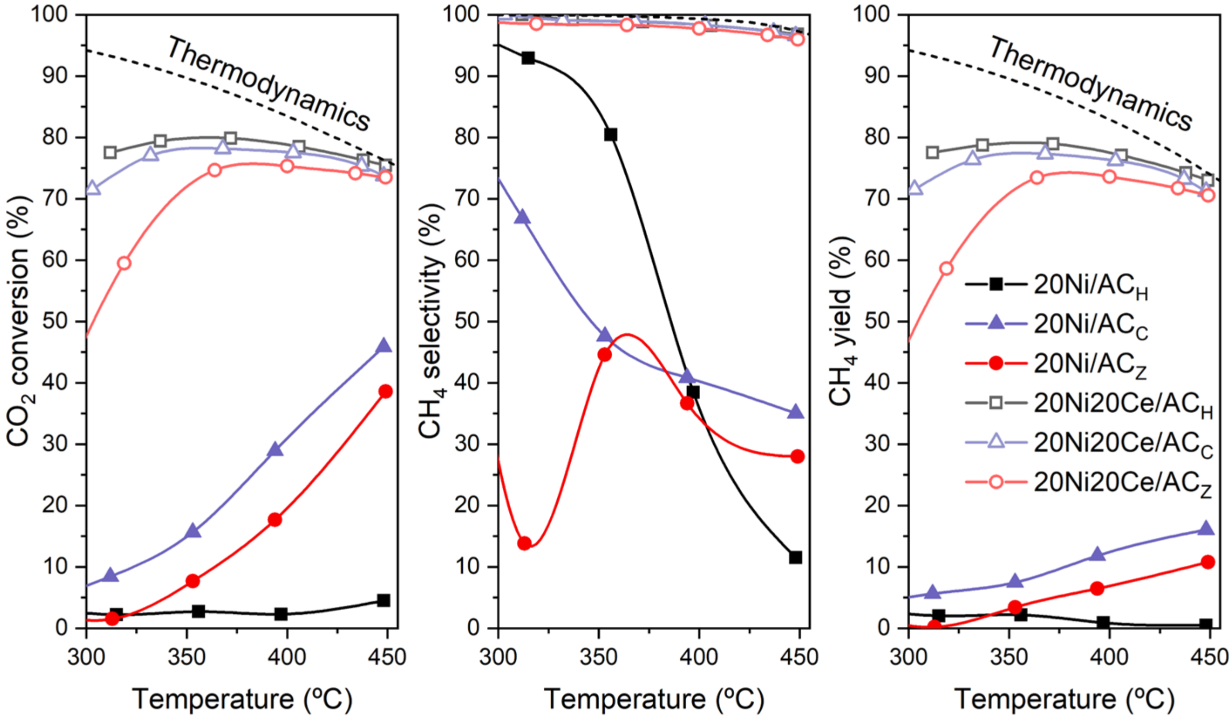

Figure 52 CO_2 conversion (%), CH_4 selectivity (%) and CH_4 yield (%) at variable temperatures for:20Ni/AC_H, 20Ni/AC_C, 20Ni/AC_Z, 20Ni20Ce/AC_H, 20Ni20Ce/AC_C and 20Ni20Ce/AC_Z. Operative conditions 1 bar, 86100 mL h^{-1} $gcat^{-1}$, CO_2:H_2:N_2 = 9:36:10.

As with monometallic nickel catalysts, the results of the XRD analysis for cerium-doped samples after catalytic tests are presented in Figure 53. Diffractograms did not show any nickel oxide formation, suggesting that no significant reoxidation occurred on nickel species during the experiments.

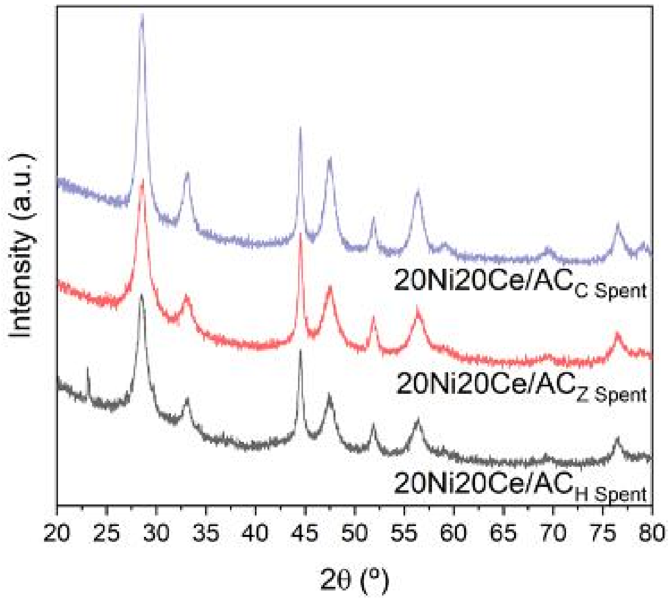

Figure 53 X-Ray diffraction of 20%Ni 20%Ce catalyst spent on the three different activated carbon

A stability test was also carried out during 9 days over 20Ni20Ce/ACC catalyst. While on day 1 and day 9 a conventional test at variable temperatures was carried out (results in Figure 54), long term experiments were run for 6 h during days 2 to 8. Indeed, 6 h-tests were run at ~350 ºC in days 2, 3, 4, 5, 6 and 8, while a test at ~250 ºC was performed on day 7 (results in Figure 55).

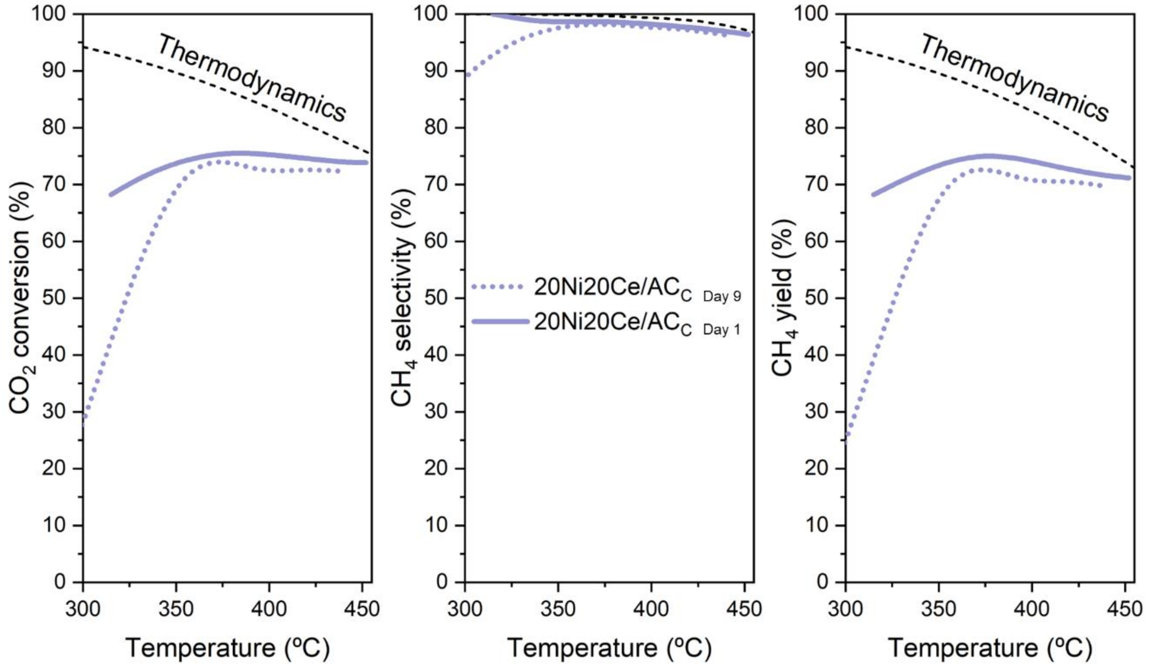

Figure 54 activity loss in terms of conversion selective and yield of 20Ni20Ce/ACc

As can be seen in Figure 54 for all three parameters, there was a decrease in catalyst activity, at least for the lower temperatures, while already from 350 °C the decrease in conversion, selectivity and yield was only a few percentage points. In fact, the stability test (Figure 55) at 350 °C shows a very low conversion loss of the catalyst over 42 hours of activity of 3% and negligible selectivity

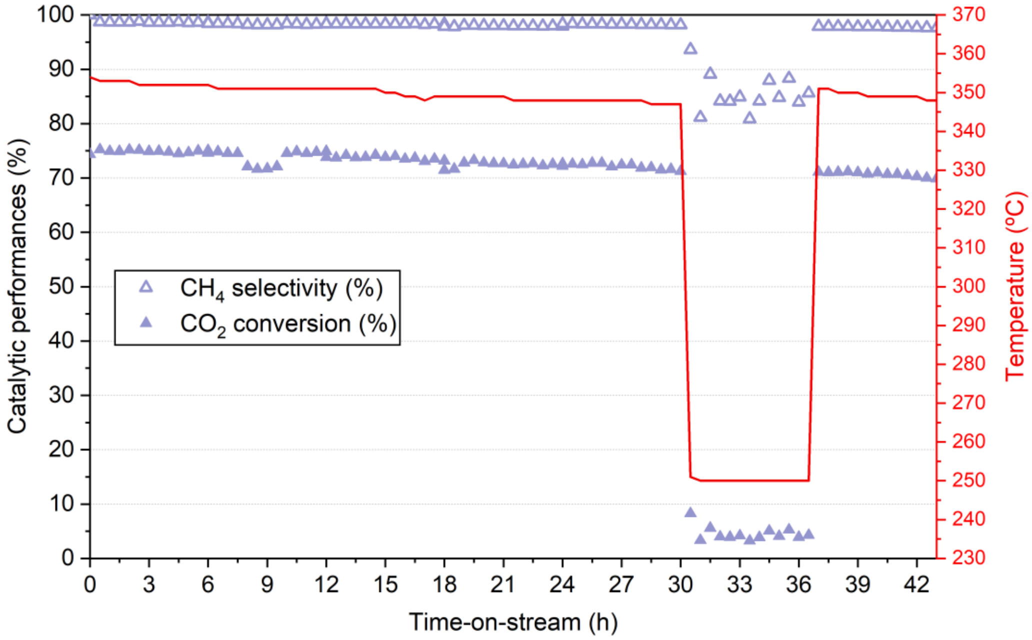

Figure 55 stability test, catalytic performance as function of time (h) and temperature (°C)

4.4 Comparison with other catalysts

Finally, the best catalyst from this work, 20Ni20Ce/AC$_C$, was compared to samples from literature in Table 4.9. All catalysts were tested at 1 atmosphere except for the (finestra et al., 2021), where a test pressure as close as possible to atmospheric pressure (3 bar) was chosen. As verified, the best catalyst from this thesis presents comparable or even better results than those from literature supported over carbons or even other type of materials such as mixed oxides.

Table 4.9 Performance of different catalysts used for methanation

Catalyst	**mL/g$_{cat}$ h**	**Temperature °C**	**Conv CO$_2$ (%)**	**Selec CH$_4$ (%)**	**References**
30Ni/Al$_2$O$_3$ 0.5SiO$_2$	**9000**	**350**	**82**	**98**	(Moghaddam et al., 2018)
30Ni/Al$_2$O$_3$	**9000**	**350**	**73**	**98**	(Moghaddam et al., 2018)
12Ni3Fe/Al$_2$O$_3$	**50000**	**420**	**84**	**100**	(Li et al., 2018)
12Ni/Al$_2$O$_3$	**50000**	**420**	**80**	**99**	(Li et al., 2018)
30Ni20Ce/Natural Kaolin	**42000**	**350**	**59**	**98**	(Aimdate et al., 2021)
40Ni10Ce/AC	**16000**	**450**	**35**	**0**	(finestra et al., 2021)
40Ni30Ce/AC	**16000**	**450**	**40**	**15**	(finestra et al., 2021)
20Ni/30Ce/AC	**16000**	**450**	**40**	**65**	(finestra et al., 2021)
15Ni/MOR	**86200**	**440**	**69**	**95**	(Bacariza et al., 2019)
15Ni/ZSM-5	**86200**	**450**	**68**	**94**	(Bacariza et al., 2019)
20%Ni20%Ce/AC$_H$	**86100**	**370**	**80**	**99**	This work

5. *Conclusion*

In this thesis, the potential of coconut shell-derived activated carbons as supports for carbon dioxide methanation reaction catalyst was analysed. For this purpose, three carbons were studied, being them synthesized by chemical and physical activation strategies. Nickel was chosen as active metal, while the role of doping the samples with Ce was also analysed.

After a preliminary characterization in terms of textural properties, the activated carbon synthesized using phosphoric acid as chemical agent was chosen to study the effect of Ni loading on the results. Results, obtained for Ni contents from 2 to 30 wt.% indicated that metallic nickel particles were larger with higher loadings and the textural properties were systematically reduced due to the blocking of the accessibility due to the metal species. Despite the particle sizes below 25 nm for all Ni loadings, none of the Ni catalysts supported over AC_H activated carbon surpassed a carbon dioxide conversion of ~5%, being this attributed to the presence of impurities in the carbon arising from the preparation step and able to poison or inhibit the active sites.

Considering an intermediate Ni loading of 20 wt.%, the other two activated carbons, prepared using $ZnCl_2$ and CO_2 for the activation, were also impregnated with nickel. In this case, the use of the activated carbon prepared by physical activation with carbon dioxide led to the best performances both in terms of conversion and selectivity, which was ascribed to the lower nickel particle size and better basicity of this sample.

Finally, NiCe catalysts with 20 wt.% Ni and 20 wt.%Ce were prepared over the three supports. Ce, in accordance with literature, was found to significantly reduce the Ni particle sizes (reductions in the order of 45-66 %) and likely improve the carbon dioxide activation capacity of the catalysts. Consequently, an improvement of the activity, especially relevant for ACH support, was observed after the addition of Ce, with conversions of ~80% at 360 ºC. The most outstanding catalyst, 20Ni20Ce/ACC, which exhibited similar or better results than other carbons and supports from literature, was also submitted to a deactivation test at variable conditions for 9 days, being the stability promising over the time.

As a result, this thesis proved the suitability of coconut shell biowastes for the synthesis of promising activated carbon supports for CO_2 methanation reaction. Considering the obtained results, complementary studies to analyse the kinetics, complete the characterization of spent samples or even analyse the mechanism over the catalysts could be potential future studies to complement the obtained results.

6. *Bibliography*

Abate, S., Mebrahtu, C., Giglio, E., Deorsola, F., Bensaid, S., Perathoner, S., Pirone, R., Centi, G., 2016. Catalytic Performance of γ-Al2O3–ZrO2–TiO2–CeO2 Composite Oxide Supported Ni-Based Catalysts for CO2 Methanation. Ind. Eng. Chem. Res. 55, 4451–4460. https://doi.org/10.1021/acs.iecr.6b00134

Abu Bakar, W.A.W., Ali, R., Toemen, S., 2012. Catalytic methanation reaction over supported nickel–ruthenium oxide base for purification of simulated natural gas. Sci. Iran. 19, 525–534. https://doi.org/10.1016/j.scient.2012.02.004

Activated Carbon [WWW Document], 2023. . Chemviron. URL https://www.chemviron.eu/products/activated-carbon/, https://www.chemviron.eu/products/activated-carbon/ (accessed 1.18.23).

Aimdate, K., Srifa, A., Koo-amornpattana, W., Sakdaronnarong, C., Klysubun, W., Kiatphuengporn, S., Assabumrungrat, S., Wongsakulphasatch, S., Kaveevivitchai, W., Sudoh, M., Watanabe, R., Fukuhara, C., Ratchahat, S., 2021. Natural Kaolin-Based Ni Catalysts for CO2 Methanation: On the Effect of Ce Enhancement and Microwave-Assisted Hydrothermal Synthesis. ACS Omega 6, 13779–13794. https://doi.org/10.1021/acsomega.1c01231

Aldana, P.A.U., Ocampo, F., Kobl, K., Louis, B., Thibault-Starzyk, F., Daturi, M., Bazin, P., Thomas, S., Roger, A.C., 2013. Catalytic CO2 valorization into CH4 on Ni-based ceria-zirconia. Reaction mechanism by operando IR spectroscopy. Catal. Today, Catalysis and synthetic fuels: state of the art and outlook 215, 201–207. https://doi.org/10.1016/j.cattod.2013.02.019

Ashok, J., Pati, S., Hongmanorom, P., Tianxi, Z., Junmei, C., Kawi, S., 2020. A review of recent catalyst advances in CO2 methanation processes. Catal. Today, VSI: EurasiaCat 356, 471–489. https://doi.org/10.1016/j.cattod.2020.07.023

Bacariza, M.C., Graça, I., Lopes, J.M., Henriques, C., 2018. Ni-Ce/Zeolites for CO2 Hydrogenation to CH4: Effect of the Metal Incorporation Order. ChemCatChem 10, 2773–2781. https://doi.org/10.1002/cctc.201800204

Bacariza, M.C., Maleval, M., Graça, I., Lopes, J.M., Henriques, C., 2019. Power-to-methane over Ni/zeolites: Influence of the framework type. Microporous Mesoporous Mater. 274, 102–112. https://doi.org/10.1016/j.micromeso.2018.07.037

Bacariza, M.C., Spataru, D., Karam, L., Lopes, J.M., Henriques, C., 2020. Promising Catalytic Systems for CO2 Hydrogenation into CH4: A Review of Recent Studies. Processes 8, 1646. https://doi.org/10.3390/pr8121646

Boudellal, M., 2018. Power-to-Gas: Renewable Hydrogen Economy for the Energy Transition, Power-to-Gas. De Gruyter. https://doi.org/10.1515/9783110559811

Carbon | Facts, Uses, & Properties | Britannica [WWW Document], 2022. URL https://www.britannica.com/science/carbon-chemical-element (accessed 2.27.23).

Dzakaria, N., Lahuri, A.H., Saharuddin, T.S.T., Samsuri, A., Salleh, F., 2021. PREPARATION OF CERIUM DOPED NICKEL OXIDE FOR LOWER REDUCTION TEMPERATURE IN CARBON MONOXIDE ATMOSPHERE 25.

finestra, C. Wheat-Straw-Derived Activated Biochar as a Renewable Support of Ni-CeO2 Catalysts for CO2 Methanation. https://doi.org/10.3390/su13168939

Fujita, S.-I., Takezawa, N., 1997. Difference in the selectivity of CO and CO2 methanation reactions. Chem. Eng. J. 68, 63–68. https://doi.org/10.1016/S1385-8947(97)00074-0

Gao, F., Tang, X., Yi, H., Zhang, B., Zhao, S., Wang, J., Gu, T., Wang, Y., 2018. NiO-Modified Coconut Shell Based Activated Carbon Pretreated with KOH for the High-Efficiency Adsorption of NO at Ambient Temperature. Ind. Eng. Chem. Res. 57, 16593–16603. https://doi.org/10.1021/acs.iecr.8b03209

Ghanbary, F., Jafarnejad, E., 2017. Removal of malachite green from the aqueous solutions using polyimide nanocomposite containing cerium oxide as adsorbent. Inorg. Nano-Met. Chem. 47, 1675–1681. https://doi.org/10.1080/24701556.2017.1357598

Jovic, V., Maksimovic, V., Pavlović, M.G., Popov, K., 2006. Morphology, internal structure and growth mechanism of electrodeposited Ni and Co powders. J. Solid State Electrochem. 10, 373–379. https://doi.org/10.1007/s10008-005-0687-1

Jurca, B., Peng, L., Primo, A., Gordillo, A., Parvulescu, V.I., García, H., 2021. Co–Fe Nanoparticles Wrapped on N-Doped Graphitic Carbons as Highly Selective CO $_2$ Methanation Catalysts. ACS Appl. Mater. Interfaces 13, 36976–36981. https://doi.org/10.1021/acsami.1c05542

Li, L., Zeng, W., Song, M., Wu, X., Li, G., Hu, C., 2022. Research Progress and Reaction Mechanism of CO2 Methanation over Ni-Based Catalysts at Low Temperature: A Review. Catalysts 12, 244. https://doi.org/10.3390/catal12020244

Li, Z., Zhao, T., Zhang, L., 2018. Promotion effect of additive Fe on Al2O3 supported Ni catalyst for CO2 methanation. Appl. Organomet. Chem. 32, e4328. https://doi.org/10.1002/aoc.4328

Lozano-Castelló, D., Lillo-Ródenas, M.A., Cazorla-Amorós, D., Linares-Solano, A., 2001. Preparation of activated carbons from Spanish anthracite: I. Activation by KOH. Carbon 39, 741–749. https://doi.org/10.1016/S0008-6223(00)00185-8

Luo, L., Wang, M., Cui, Y., Chen, Z., Wu, J., Cao, Y., Luo, J., Dai, Y., Li, W.-X., Bao, J., Zeng, J., 2020. Surface Iron Species in Palladium–Iron Intermetallic Nanocrystals that Promote and Stabilize CO2 Methanation. Angew. Chem. Int. Ed. 59, 14434–14442. https://doi.org/10.1002/anie.201916032

Martin, N.M., Hemmingsson, F., Schaefer, A., Ek, M., Merte, L.R., Hejral, U., Gustafson, J., Skoglundh, M., Dippel, A.-C., Gutowski, O., Bauer, M., Carlsson, P.-A., 2019. Structure-function relationship for CO2 methanation over ceria supported Rh and Ni catalysts under atmospheric pressure conditions. Catal. Sci. Technol. 9, 1644–1653.

Mebrahtu, C., Krebs, F., Abate, S., Perathoner, S., Centi, G., Palkovits, R., 2019. Chapter 5 - CO2 Methanation: Principles and Challenges, in: Albonetti, S., Perathoner, S., Quadrelli, E.A. (Eds.), Studies in Surface Science and Catalysis. Elsevier, pp. 85–103. https://doi.org/10.1016/B978-0-444-64127-4.00005-7

Moghaddam, S.V., Rezaei, M., Meshkani, F., Daroughegi, R., 2018. Synthesis of nanocrystalline mesoporous Ni/Al2O3SiO2 catalysts for CO2 methanation reaction. Int. J. Hydrog. Energy 43, 19038–19046. https://doi.org/10.1016/j.ijhydene.2018.08.163

Mohamad Nor, N., Lau, L.C., Lee, K.T., Mohamed, A.R., 2013. Synthesis of activated carbon from lignocellulosic biomass and its applications in air pollution control—a review. J. Environ. Chem. Eng. 1, 658–666. https://doi.org/10.1016/j.jece.2013.09.017

Molino, G., Gandiglio, M., Fiorilli, S., Lanzini, A., Drago, D., Papurello, D., 2022. Design and Performance of an Adsorption Bed with Activated Carbons for Biogas Purification. Molecules 27, 7882. https://doi.org/10.3390/molecules27227882

Omri, A., Benzina, M., 2012. CHARACTERIZATION OF ACTIVATED CARBON PREPARED FROM A NEW RAW LIGNOCELLULOSIC MATERIAL: ZIZIPHUS SPINA-CHRISTI SEEDS.

Omri, A., Benzina, M., Ammar, N., 2013. Preparation, modification and industrial application of activated carbon from almond shell. J. Ind. Eng. Chem. 19, 2092–2099. https://doi.org/10.1016/j.jiec.2013.03.025

(PDF) Gas Sorption System Operating Manual [WWW Document], n.d. . dokumen.tips. URL https://dokumen.tips/documents/gas-sorption-system-operating-manual.html (accessed 2.1.23).

Pelicano, C.M., Rapadas, N.J., Magdaluyo, E., 2017. X-ray peak profile analysis of zinc oxide nanoparticles formed by simple precipitation method. AIP Conf. Proc. 1901, 020016. https://doi.org/10.1063/1.5010453

Pirola, C., Galli, F., Patience, G.S., 2018. Experimental methods in chemical engineering: Temperature programmed reduction-TPR. Can. J. Chem. Eng. 96, 2317–2320. https://doi.org/10.1002/cjce.23317

Punti di Fusione dei Metalli | La Terra e il Fuoco [WWW Document], n.d. URL https://www.giovannabellinigioielli.com/punti-di-fusione-dei-metalli (accessed 2.11.23).

Russo, N., 2022. catalysis course.

Schaaf, T., Grünig, J., Schuster, M.R., Rothenfluh, T., Orth, A., 2014. Methanation of CO2 - storage of renewable energy in a gas distribution system. Energy Sustain. Soc. 4, 2. https://doi.org/10.1186/s13705-014-0029-1

Schmider, D., Maier, L., Deutschmann, O., 2021. Reaction Kinetics of CO and CO2 Methanation over Nickel. Ind. Eng. Chem. Res. 60, 5792–5805. https://doi.org/10.1021/acs.iecr.1c00389

Sharma, S., Hu, Z., Zhang, P., McFarland, E.W., Metiu, H., 2011. CO2 methanation on Ru-doped ceria. J. Catal. 278, 297–309. https://doi.org/10.1016/j.jcat.2010.12.015

Sietsma, J.R.A., Jos van Dillen, A., de Jongh, P.E., de Jong, K.P., 2006. Application of ordered mesoporous materials as model supports to study catalyst preparation by impregnation and drying, in: Gaigneaux, E.M., Devillers, M., De Vos, D.E., Hermans, S., Jacobs, P.A., Martens, J.A., Ruiz, P. (Eds.), Studies in Surface Science and Catalysis, Scientific Bases for the Preparation of Heterogeneous Catalysts. Elsevier, pp. 95–102. https://doi.org/10.1016/S0167-2991(06)80895-5

Specchia, S., 2022. Multiphase equipment design's course, 2022nd ed. Torino.

Strucks, P., Failing, L., Kaluza, S., 2021. A Short Review on Ni-Catalyzed Methanation of CO2: Reaction Mechanism, Catalyst Deactivation, Dynamic Operation. Chem. Ing. Tech. 93, 1526–1536. https://doi.org/10.1002/cite.202100049

Suhas, Carrott, P.J.M., Ribeiro Carrott, M.M.L., 2007. Lignin – from natural adsorbent to activated carbon: A review. Bioresour. Technol. 98, 2301–2312. https://doi.org/10.1016/j.biortech.2006.08.008

Sun, D., Siddiqui, M.O.R., Iqbal, K., 2019. 4 - Specialty testing techniques for smart textiles, in: Smith, W.C. (Ed.), Smart Textile Coatings and Laminates (Second Edition), The Textile Institute Book Series. Woodhead Publishing, pp. 99–116. https://doi.org/10.1016/B978-0-08-102428-7.00004-3

Swalus, C., Jacquemin, M., Poleunis, C., Bertrand, P., Ruiz, P., 2012. CO2 methanation on Rh/γ-Al2O3 catalyst at low temperature: "In situ" supply of hydrogen by Ni/activated carbon catalyst. Appl. Catal. B Environ. 125, 41–50. https://doi.org/10.1016/j.apcatb.2012.05.019